

# Mapping hydrothermal gold mineralization using Landsat 8 data. A case of study in Chaves license, Portugal

Rui Mateus da Cunha Frutuoso

Mestrado em Geologia

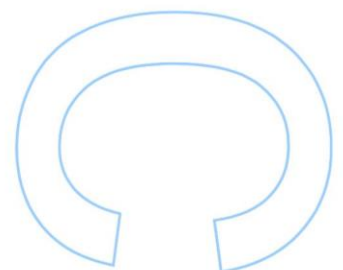
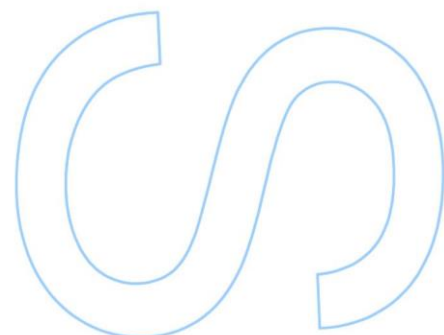
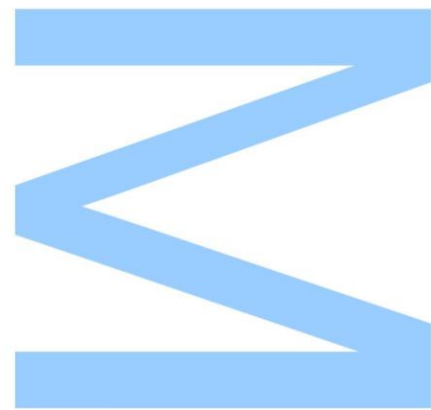
Departamento de Geociências, Ambiente e Ordenamento do Território  
2015

## **Orientador**

Alexandre Martins Campos de Lima, Professor auxiliar  
Faculdade de Ciências da Universidade do Porto

## **Co-orientador**

Ana Cláudia Moreira Teodoro, Professor auxiliar  
Faculdade de Ciências da Universidade do Porto

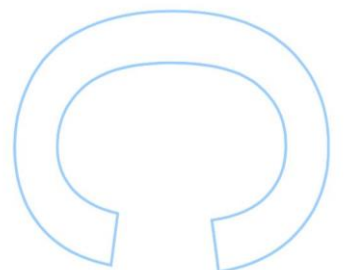
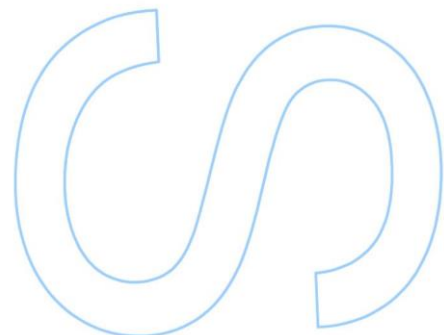
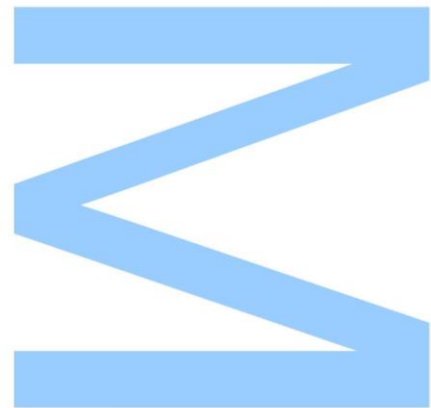






Todas as correções determinadas pelo júri, e só essas, foram efetuadas.  
O Presidente do Júri,

Porto, \_\_\_\_/\_\_\_\_/\_\_\_\_





*"We must preach up traveling (...) as the first, second, and third  
requisites for a modern geologist"*

Charles Lyell



# Acknowledgments

I would like to thank Medgold Resources Corp. to accepted this project and providing all the information, and particularly to Daniel James for the opportunity to work in this company.

Thanks must also go to NASA and USGS for providing the Landsat 8 data used in this study.

My thanks to Prof. Dr. Alexandre Lima and Prof. Dr. Ana Claudia Teodoro for the invitation and trust to carry out this project. Thank you also for the support and guidance throughout this project.

To the Faculty of Science of the University of Porto and all the teaching and non-teaching staff of the Department of Geosciences, Environment and Spatial Planning.

A recognition to my colleagues for all fruitful discussions, advices and moments in the field.

Thanks to Rob Selwyn for the English revising and being always available to help.

To my friends by words of encouragement.

To Maria by the unconditional support.

To my brothers.

And a special thanks to my parents for all the effort, sacrifice, and support. This work is also yours.

# Abstract

A geological based remote sensing study was carried out over the Chaves License in northern Portugal. In this study, Landsat 8 imagery was used in order to map hydrothermal alteration associated with gold mineralization.

The Chaves license is an area acquired by Medgold resources Corp. for gold exploration. This license is located in the Trás-os-Montes region, in Portugal, covering an area over 600 Km<sup>2</sup>, where gold exploration dates back to the Roman era with several mining and exploration works. Geologically, this study area is within the Galician Trás-os-Montes Zone, and it's composed of Hercynian granites that intruded and metamorphozed Silurian sediments. Gold mineralization consists in quartz veins with disseminated sulfides or in massive sulfide veins, where gold is generally associated with the arsenopyrite and pyrite as native gold or *electrum*. These mineralized structures are NE trending and are usually found within altered granite.

Different remote sensing techniques, such as single band combinations, band ratio and principal component analysis, were applied in order to identify geological features. The generation of a target exploration map was made possible by the culmination of hydrothermal mapping, structural mapping and analysis and historical data. New generated data provide a useful insight for further exploration.

**Keywords:** Remote sensing, Landsat, gold, exploration, hydrothermal alteration



## Resumo

Foi realizado um estudo de deteção remota na licença de prospeção e pesquisa de Chaves no Norte de Portugal. Neste estudo foi utilizado imagens *Landsat 8* de forma a mapear zonas de alteração hidrotermal associada a mineralizações auríferas.

A licença de Chaves foi adquirida pela empresa Medgold Resources Corp. para a prospeção de ouro. Esta licença localiza-se na região de Trás-os-Montes englobando uma área de 600 Km<sup>2</sup>, onde a prospeção de ouro remonta a era Romana sendo conhecidos vários trabalhos mineiros e de pesquisa. Geologicamente, esta área localiza-se na Zona geotectónica Galiza Trás-os-Montes, sendo composta por granitos Hercínicos que intruíram e metamorfizaram sedimentos do Silúrico. A mineralização aurífera corresponde a filões de quartzo com sulfuretos disseminados ou filões de sulfuretos maciços, onde o ouro geralmente está associado à arsenopirite e pirite onde ocorre como ouro nativo ou *electrum*. Estas estruturas mineralizadas têm uma orientação para NE e geralmente ocorrem em granito alterado.

Foram utilizadas diversas técnicas de deteção remota, como a combinação de bandas, *band ratio* e a análise de componentes principais, de forma identificar certos aspetos geológicos. A criação de um mapa com alvos de prospeção foi conseguida com base na combinação do mapeamento de alteração hidrotermal, de estruturas geológicas e na análise de dados históricos. A geração destes novos dados permite fornecer novas indicações para os próximos programas de prospeção.

**Palavras-Chave:** Deteção remota, *Landsat*, ouro, prospeção, alteração hidrotermal



## List of figures

Figure 1 – Study area location and road connection. ....	21
Figure 2 - Elevation model and streams from the studied area. ....	23
Figure 3 - Subdivisions in zones of the Iberian Massif, according Lotze (1945), Julivert et al. (1972) and Farias et al. (1987). (Adapted from Vera, J. A., 2004). .....	28
Figure 4 - Main deformation events in the Iberian Peninsula during the Hercynian orogeny (Dias e Ribeiro, 1995).....	30
Figure 5 - Geological map of the study area.....	32
Figure 6 - Gold occurrences in northern Portugal.....	33
Figure 7 – Structural evolution of Bobabdela, Limarinho and Poço das Freitas sector. (Adapted from Griveaud and Dixsaut (1989). Stage 1 – N-S shear zones with left movement affect N60° shear zones. Stage 2 and stage 3 – N60° sinistral shears created an extensional zone at the intersection of the two strike-slip faults. These extensional zones acted as a conduit for the fluids, forming quartz veins which followed the formation of hydraulic breccia mineralized with hematite. Occurred the installation of N30-N40° quartz veins with arsenopyrite. Stage 4 – Intensification of the movement result in a denser parallel network of mineralized veins in the center of dilation zones. Stage 5 – End of mineralizing fluids. Emplacement of milky quartz veins, sterile or weakly mineralized, with N60° trend at Limarinho and Sapelos. Stage 6 – Changing in the shortening direction, from N60° to N-S, resulting in new openings with infillings of white quartz. Normal and/or sinistral movement in N-S TO N20° faults at south of Limarinho caused offset of mineralized structures at Poço das Freitas. Sinistral movement of the Sapelos fault caused brecciation of the vein. ....	36
Figure 8 – Actual structural stage of Bobabdela, Limarinho and Poço das Freitas sector. (Adapted from Griveaud and Dixsaut (1989). Late brittle stage with the shortening direction N140°E (1), allowing the sinistral movement in the N-S faults (2) which accentuates the offset of mineralized structures. ....	37
Figure 9 – (A) Laboratory spectra of alunite, chlorite, kaolinite, muscovite, calcite, and epidote. (B) Laboratory spectra of limonite, jarosite, hematite and goethite (Clark et al., 1993).....	46

Figure 10 - True Colour image. RGB combination of bands 4, 3, 2. Green colour represent vegetation, brown and brown represent soil or rock and blue water. 50

Figure 11 – False Colour Composite. RGB combination of bands 5, 4, 3. Red colour represent vegetation, black represent water and rock or soil are represented by greyish colour. This RGB combination highlights the boundaries between vegetated and outcrop areas. .... 51

Figure 12 - RGB combination for bands 7, 5, 2. Enhanced image where outcrops are represented in shades of orange and red, Vegetation in light green and water in black. .... 52

Figure 13 – RGB combination for bands 5, 6, 7. In this image vegetated areas appear in orange colour, outcrops in light blue and water in black. Some hydrothermal altered rocks can be identified as blue. .... 53

Figure 14 – (a) Landsat 8 band ratio 4/2 image reveals areas where iron minerals (hematite, goethite, limonite, etc.) are abundant shown in bright tones; (b) Landsat 8 band ratio 6/5 image discriminates ferrous minerals with bright tone. (c) Landsat 8 band ratio (7/5) image reveals clay minerals, as illite, kaolinite and montmorillonite. (d) Landsat 8 band ratio 6/7 image shows alunite and hydrothermal clay minerals..... 54

Figure 15 - Sabin's ratio image (4/2, 6/7, 6/5). Outcrops are represented in light blue-yellow colour, vegetation in blue and water in dark green. Strong yellow represent buildings and other human constructions and light green altered rocks. .... 55

Figure 16 –Band ratio of 4/2, 6/7, 5, in RGB. Outcrops are identified as rose and light brown, vegetation as light blue and water as black. Urbanized areas are highlighted as strong rose. .... 56

Figure 17 - Kaufmann ratio (7/5, 5/4, 6/7). This band ratio combination highlight metasediments as dark green and granite outcrops are represented as rose, vegetation as light blue and water as red. Some red areas can be related to the hydrothermal alteration..... 57

Figure 18 - RGB colour combination of Principal Component Analysis 1, 2, 3 components. Green-yellow colours represent granite outcrops, vegetation in purple, water as light blue and metasediments as blue. .... 59

Figure 19 – Principal Component image from Landsat 8 data for iron oxides minerals (PC4) as bright pixels.....	61
Figure 20 - Principal Component image from Landsat 8 data for hydroxyl bearing minerals (PC4) as bright pixels.....	63
Figure 21 – RGB combination using hydroxyl bearing image, hydroxyl and iron oxide bearing image, and iron oxide bearing image. This composite map the hydrothermal alteration areas.....	64
Figure 22 - Lithological map based on Landsat 8 imagery analysis. ....	66
Figure 23 – Structural pattern defined based on Landsat 8 imagery and terrain analysis. ....	67
Figure 24 - Hydrothermal alteration areas in and around Chaves license.....	68
Figure 25 - Hydrothermal alteration map with Au anomalous basins for Chaves License.....	69
Figure 26 - Target exploration map .....	71

## List of tables

Table 1 – Vertex coordinates of Boticas License.....	24
Table 2 – Vertex coordinates of Chaves license. Between vertex 1 and 18 fallow the border line between Portugal and Spain.....	25
Table 3 - Landsat systems, operational dates and sensors. In Markham 2012.	40
Table 4 – OLI and TIRS bands characteristics. (USGS, 2015a).....	41
Table 5 - Eigenvectors and eigenvalues of PCA on Landsat 8 imagery. ....	58
Table 6 – Eigenvectors and eigenvalues for Principal Components of Landsat 8 bands 2, 4, 5, and 6 for iron oxides minerals.....	60
Table 7 - Eigenvectors and eigenvalues for Principal Components of Landsat 8 bands 2, 5, 6, and 7 for Hydroxyl bearing minerals. ....	62

# Table of contents

1. <i>Introduction</i>	18
1.1. Remote sensing	19
2. <i>General description</i>	21
2.1. Location	21
2.2. Physiography	22
2.3. Description of Property	24
2.4. Historical Background	25
3. <i>Geological Setting</i>	28
3.1. Regional Geology	28
3.2. Local Geology	31
3.3. Gold Mineralization	33
3.3.1. Local Gold Mineralization	35
3.3.2. Structural Control of gold mineralization	35
3.4. Fluid chemistry & P-T conditions	37
4. <i>Data &amp; Image Processing Methods</i>	39
4.1. Data	39
4.1.1. Geological Data	39
4.1.2. Landsat data	39
4.1.3. GIS Software	42
4.2. Image Processing	43
4.2.1. Pre-processing	43
4.2.2. Image Processing Methods	44
4.2.2.1. Single Band Combinations	44
4.2.2.2. Band Ratio	45
4.2.2.3. Principal Components Analysis (PCA)	47
5. <i>Results and Interpretations</i>	49
5.1. Image Analysis	49
5.1.1. Single Band Combinations	49
5.1.2. Band Ratio	53
5.1.3. Principal Component Analysis (PCA)	58
5.2. Feature Extraction	64
5.2.1. Lithologic Mapping	64
5.2.2. Structural Mapping	67

5.2.3. Hydrothermal Alteration Mapping	68
5.3. Target Exploration Map	70
6. <i>Conclusions</i>	72
7. <i>Further Work</i>	74
8. <i>References</i>	76





# 1. Introduction

Geological remote sensing has proved itself as an important tool to locate mineral deposits by, recognizing processes of mineralization through spectral anomalies (Sabins, 1999; Rajesh, 2004; van der Meer *et al.* 2012). Remote sensing is a powerful technique in identifying hydrothermally altered rocks, structures, lineaments, oxidation products, morphology, lithological units, vegetation anomalies and other valuable information to geologists (Goetz *et al.*, 1982; Sabins, 1999; Drury, 2001; Goetz, 2009). Regional mapping of exposed altered rocks with remote sensing is a useful complement for geological field exploration, allowing a first approach in terrain recon, providing valuable information of a study area, that otherwise were not available (Sabins, 1999).

Remote sensing data combined with geological data, such as geochemical, lithological, and structural, can be useful to create mineral potential maps defining exploration targets. Geographic Information System (GIS) environment is used for this combination and analysis of spatial data, as it is an efficient tool to manage different contents and apply algorithms to determine these potential areas for mineral exploration.

The work described in this dissertation was developed during an internship with Medgold Resources Corp., a TSX-V listed Resource Company, part of Vancouver based Gold Group. Medgold holds several licenses in Portugal and Spain with a main focus on gold exploration. In July 2013, Medgold acquired the Boticas License by *Direcção Geral de Energia e Geologia* (DGEG), and later in August 2015, the Chaves license. The Boticas license covers an area with 106.52 Km<sup>2</sup> and lies inside Chaves license covering 495.18 Km<sup>2</sup>. These two licenses are the study area in this work.

The Chaves license is located in parautochthonous terrane of Galicia-Trás-os-Montes Zone. The principal geological unit in this area is a two-mica granite that intruded into Silurian metasediments. This is associated with the Hercynian orogeny caused by the late Palaeozoic continental collision and consequently the formation of supercontinent Pangea.

Vestiges of gold mining in this region have been identified since Pre-Roman civilizations, but the major and more relevant works were done by the Romans. Several archaeological sites are found in this region associated to roman activity (Viegas and

Martins, 1992; COGEMA, 1990; Martins, 2005; Mendonça, 2006; Lima *et al.*, 2014). Three important exploitations are identified as roman gold mines, so-called as Limarinho, Poço das Freitas and Batocas. In recent times, diverse exploration companies carried out exploration programs through this region, which include soil sampling, channel sampling and diamond drilling.

Gold mineralization in the study area is hosted in quartz veins in granites, and it is believed that is controlled by a large-scale regional fault – Régua-Verín Fault – a structural feature common in many large-scale orogenic gold deposits (COGEMA, 1990; Harford *et al.*, 1998). This Régua-Verín fault is NNE trending and cuts through the concession area, striking greater than 200 km in length. The mineralization may be a major dilatational zone, typical of orogenic gold systems (COGEMA, 1990; Harford *et al.*, 1998; Mendonça, 2006). Gold bearing quartz veins are NE striking, typically sub-vertical, sub-parallel to en-echelon, with thickness ranging from millimetres to tens of centimetres. Mineralization is associated with arsenopyrite, and as free gold or electrum (COGEMA, 1990; Harford *et al.*, 1998; Mendonça, 2006; Cepedal *et al.*, 2013). Granite alteration is directly related with the installation of these veins. This granite alteration occurs in concentrated zones of quartz veining and Romans selectively mined these areas (Harford *et al.*, 1998; Mendonça, 2006).

The Chaves license is extensive and previous companies focused their exploration programs on a small portion where the mineralization was known. This region is not extensively studied or explored, so there is a weak understanding about the occurrence of gold mineralization and emplacement in this region. In order to identify new gold occurrence potential areas, a remote sensing approach was applied using Landsat 8 OLI multispectral imagery. Landsat 8 OLI imagery was analysed in a GIS environment by applying different image processing techniques that effectively identified hydrothermal alteration zones based on mineral spectral signatures. The results were interpreted and spatial analysis tools were used in order to define new target areas for future fieldwork explorations.

## 1.1. Remote sensing

Sabins (1999) describe remote sensing as “the science of acquiring, processing, and interpreting images and related data, acquired from aircraft and satellites that record the interaction between matter and electromagnetic energy”. In mineral exploration,

remote sensing it is an important tool for regional mapping, structural interpretation, and recognize hydrothermally altered rocks by their spectral signatures.

In the last decades, geological remote sensing has proved to be a great tool in mineral exploration. Many ore deposits have been recognized using satellite imagery (Sabins, 1999; van der Meer, 2012; Pour & Hashim, 2015). Geologists developed techniques and analysis methods to digitally process satellite images and recognize hydrothermal alteration areas. Several studies showed the potential of remote sensing for mapping hydrothermally altered rocks. Moradi *et al.* (2015) created a mineral prospectivity map for gold mineralization based in ASTER imagery in Central Alborz, Iran; Han and Nelson (2015), used Landsat 8 imagery to map the regional distribution of hydrothermal alteration in zones of northwestern British Columbia, based on spectral unmixing image analysis. Pour and Hasim (2015) map hydrothermal alteration areas and lithological units in Sar Chseshmeh Copper mining district, south-eastern of Iran, using Landsat 8 imagery. Zoheir and Emam (2012) map gold exploration targets in South Eastern Desert, Egypt using ASTER and Landsat ETM+ imagery.

The spectral signature identification of minerals and assemblage of minerals formed by hydrothermal alteration, are used to identify patterns of outflows of hydrothermal systems, which can allow recognition of mineralized zones (Sabins, 1999; Rajesh, 2004; Moradi *et al.*, 2015). Spectral signatures of minerals and rocks have the basis on the work done by Hunt (1977) and after Salisbury *et al.* (1989), that measured in laboratory the spectra of several different minerals and rocks (spectral signature). This technical information is critical for the interpretation of remotely sensed data. The United States Geological Survey (USGS) provides a spectral library with spectral reflectance of hundreds of materials measured in laboratory (Clark *et al.*, 2007). Spectral signatures obtained by Landsat imagery are different when compared to the laboratory measurements, due pixel resolution and the presence of different materials in one pixel.

## 2. General description

### 2.1. Location

This concession is situated in Northern Portugal, at Trás-os-Montes region, approximately 150km northeast of Porto, in the Vila Real district and includes the municipalities of Chaves, Boticas, Montalegre and Valpaços (Figure 1).



Figure 1 – Study area location and road connection.

The main town in this area is Chaves, and is located proximal to the centre of the concession. A good road network facilitate the access to all of the concession area. Non-pavement roads, in good conditions for car circulation give access to the roman works, outcrops, etc.

Local economy is strongly in agricultural and the demography indicates an aging population. The local population and administration are supportive of resource development and exploration programs.

In this area there are several archaeological occurrences from pre-Roman era. Mining works are a great expression of the Roman presence in this region, like Limarinho, Poço das Freitas and Batocas. These works, consists in open pit and rare underground works located near Boticas.

## 2.2. Physiography

The climate in this region is temperate with considerable thermal amplitude. Winter season is cold with high precipitation and summers includes temperatures that can reach 40°C. Snowfalls only occurs at higher elevations and last for a short period time (Climate-data.org, 2014).

The topography is mountainous with deep valleys (Figure 2). In this region, the altitudes range between 270m, at Terva river, to 1155m, in “Serra do Leiranco” at the western side of the concession. A valley with a strike NNE-SSW, was formed by Régua-Verín fault that, cross this concession area. The Régua-Verín fault has a lateral strike that runs along 200km from Penacova to Verín (Cabral, 1995). Consists in an active fault system that express reactivations with diverse thermal occurrences along the extension (Cabral, 1995; Harford *et al.*, 1998).

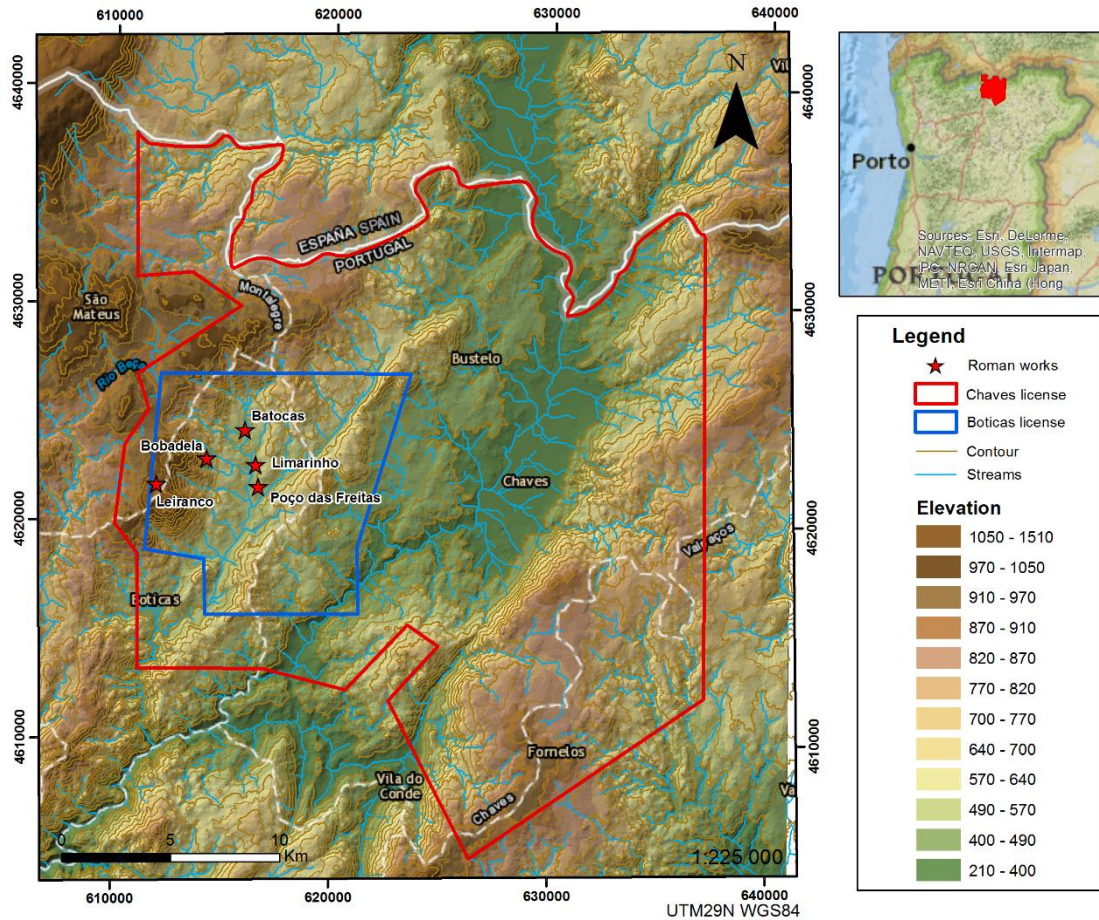


Figure 2 - Elevation model and streams from the studied area.

An extensive stream network, that include Tâmega, Terva and Beça rivers and other small tributaries, cut this study area and conditioned the morphology. They show a general orientation NNE-SSW, NE-SW, and NW-SE whereby these orientations are related with the post-Hercynian fracturing.

The concession area covers the topographic maps nº20, 21, 22, 33, 34, 35, 46, 47, 48 and 61 with a scale 1:25000 from military geographical services (IGEOEMilitary Geo-Spatial Information Center). Using these maps, it possible to notice an orientation of the elevations with a NNE-SSE trend, possibly related with a strong structural and lithological control on geomorphology of this region.

### 2.3. Description of Property

Medgold acquired the Boticas exploration license from *Direção-Geral de Energia e Geologia* (DGEG) of Portugal in July 2013. This concession covers an area with 106,5Km<sup>2</sup> delineated by a polygon with coordinates PT-TM06/ETRS89 (European Terrestrial Reference System 1989), showed in Table 1:

Table 1 – Vertex coordinates of Boticas License.

Boticas License		
Vertex	X(m)	Y(m)
1	41500,683	226499,384
2	41557,622	223964,433
3	48576,422	223983,349
4	48507,793	227035,186
5	50986,311	235002,957
6	39525,552	235012,155
7	38785,764	226936,828

Later, in August 2015, Medgold acquired the Chaves license, covering 495 Km<sup>2</sup>. This license area is delimited by a polygon with the vertex, in coordinates PT-TM06/ETRS89 (European Terrestrial Reference System 1989), showed in Table 2.



Table 2 – Vertex coordinates of Chaves license. Between vertex 1 and 18 follow the border line between Portugal and Spain.

Chaves License		
Vertex	X(m)	Y(m)
1	64516,889	241523,655
2	64502,315	220325,287
3	53736,071	212986,374
4	50036,169	220227,268
5	52322,889	222727,585
6	50910,824	223694,266
7	48075,927	220707,191
8	44245,416	221698,971
9	38527,457	221699,860
10	38527,355	226977,823
11	37483,336	228347,793
12	37969,262	231983,776
13	39056,414	233616,803
14	38557,195	235228,765
15	43291,101	238333,834
16	41039,087	239885,780
17	38528,109	239685,732
18	38526,963	247205,860

These two concessions are the study area in this present work. It will referred as one unit as the Boticas concession is located within the Chaves license.

## 2.4. Historical Background

Mining history in this region dates to pre-Roman times, but during the Roman era mineral exploitation was more intense and industrial. Romans extracted a diversity of metals from Iberia such, as gold, silver, cooper and iron (Carvalho and Ferreira, 1954; Matias, 2004; Mendonça, 2006). During the 450 year occupation of Iberia by the Romans, it has been estimated that more than 40 million ounces of gold were produced from northwest Spain and northern Portugal from alluvial, eluvial and hard rock deposits (Harford *et al.*, 1998). Roman mining in northern Portugal was from rock quartz vein deposits associated eluvium and alluvium, and oxidized and supergene enrichment zones of massive sulfide deposits (Pereira and Meireles, 1998, Mendonça, 2006).

During the Moors occupation, the gold exploitation in Iberia was basically alluvial gold. After the Moors occupation, Iberia was not recognized a gold mining culture (Harford, 1998; Mendonça, 2006).

This concession area was intensely mined in the past, with several visible works most of them from Roman period (see references in Lima *et al.*, 2011). There are a lot of mining evidences and small villages dispersed in the entire research area. The Boticas license include three principal Roman works, that consist in open pits where quartz veins hosted in granitic rocks were mined such as: Limarinho, Poço das Freitas and Batocas.

Gold exploration was based on systematic empiric criteria application that consisted in panning sediments along rivers (Mendonça, 2006; Lima *et al.*, 2014). If positive results occurred, the area was searched along the stream to search for the main deposit. For study and evaluation of mineralization, galleries and shafts were opened (Matias 2004, Lima *et al.*, 2014). In case of potential discovery of a deposit, the potential area was mined in open pit by using hydraulic methods known as Arrugia or Ruína Montium, depending on lithology and deposit characteristics (Matias, 2004; Mendonça, 2006).

From 1987 to 1991 COGEMA (Compagnie Générale des Matières Nucléaires de France) acquired a concession in this area and conducted an extensive exploration program, including soil sampling, rock sampling, mapping, trenching and, diamond drilling. In conclusion of this exploration approach, COGEMA identified 15 gold occurrences, but only three were drill tested.

In 1997 Minas Romanas – Sociedade Mineira, Lda acquired a concession in this area where they conducted an exploration program based on rock chip sampling and a stream sampling by the method BLEG (Bulk Leach Extractable Gold). This exploration program consisted in delineate known and unknown gold anomalies, principally the invisible gold deposits not exploited by romans.

Kernow Resources & Developments Inc., held a license for exploration in this area from 2006 to 2008. Kernow drilled several targets in Limarinho, and other explorations works, including chip and channel sampling.

Medgold started an exploration program for the Boticas concession at the beginning of 2015, which included a soil and rock chip sampling campaign, and also a geological mapping and geophysics (Magnetic survey) campaign. Data compilation and

analysis from previous works has been done in way to collect all information available and to ensure consistency when using historical data.

### 3. Geological Setting

#### 3.1. Regional Geology

During the long diverse history of earth, different orogenies have sculpted geology of which is visible today. The Hercynian or Variscan orogeny consists of an important that was the result of the collision between Laurussia and Gondwana (closure of the Rheic ocean), that affected what is now Europe including the Iberian Peninsula. This orogeny formed a belt of deformation called the Ibero-Armorican arc (Oliveira, 2001; Matte, 1986, 1991; Ribeiro *et al.*, 2007; Vigneresse, 1999; Dias *et al.*, 1995). This orogeny occurred along de Devonian (390Ma) to Carbonic (290/280Ma) period (Dias and Ribeiro, 1993, 1995; Ribeiro *et al.*, 1995; Matte, 1986, 1998, 2001; Fernández *et al.*, 2003). The Chaves concession is located on the occidental portion of the European Hercynian belt, in the Iberian Massif.

The Iberian Massif is limited in the west by the Atlantic Ocean whereas the east is covered by Mesozoic and Tertiary terranes. The Biscay gulf is situated northwards from the Iberian Massif and the Alpine belt lies SE with segments of The Iberian Massif containing a complex structure that develops with a WNW-ESE orientation. Lotze (1945)

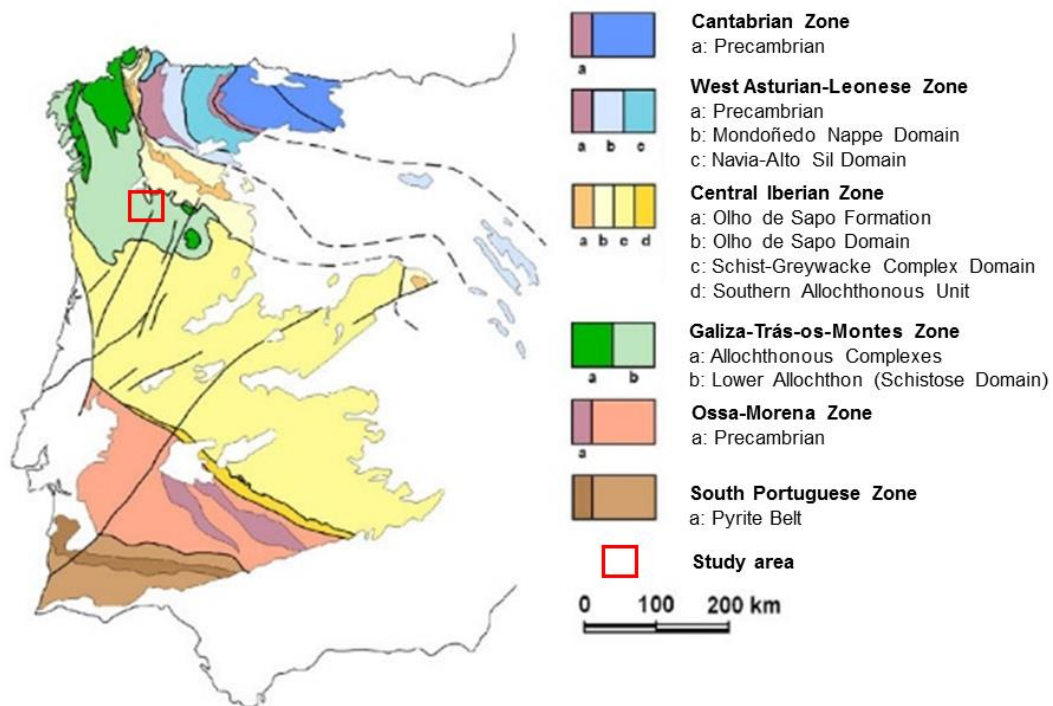


Figure 3 - Subdivisions in zones of the Iberian Massif, according Lotze (1945), Julivert *et al.* (1972) and Farias *et al.* (1987). (Adapted from Vera, J. A., 2004).

developed a division of the Iberian Massif in different geotectonic zones with different paleogeographic, tectonic, metamorphic and plutonic characteristics parallel to the structural alignments of the Hercynian orogeny. Julivert *et al.*(1972) based on the work of Lotze, reevaluated these geotectonic zones to establish the newly-accepted zones (Figure 3). These zones are denominated as: Cantabric zone (CZ), West Asturico-Leonesa zone (WALZ), Central Iberian Zone (CIZ), Ossa Morena Zone (OMZ), and South Portuguese Zone (SPZ). Later Farias *et al.* (1987) define a new Zone, the Galician-Trás-os-Montes Zone (GTMZ).

This geotectonic organization results from three main ductile deformation phases (D1, D2 and D3) that acted during the Hercynian orogeny and several post-D3 phases (Figure 4) (Ribeiro, A., 1974, 2013; Noronha *et al.*, 1979; Dias e Ribeiro, 1995; Noronha *et al.*, 2006). These three phases are responsible by the foliations in the deformed rocks.

The D1 phase is characterized by the formation of large folds with different vergence and orientations in autochthonous, allochthonous and parautochthonous. These folds present a NW-SE trending orientation with a sub-vertical axial plane in autochthonous (CIZ) and slightly vergent in the parautochthonous (Noronha *et al.*, 2006). Stratigraphical and geochronological data date the first Hercynian stage as medium Devonian (Ferreira *et al.* 1998)

The second phase of deformation, D2, succeeded the D1 phase and accentuates the vergence to SE, forming overturned folds with a short inverse limb and a sub-horizontal shear cleavage. This stage is represented principally in the allochthonous and parautochthonous (Noronha *et al.*, 2006).

The third phase of deformation, D3, (300±10Ma) is present in all of the terranes (Autochthonous, Allochthonous and Parautochthonous) where D3 developed large open folds with sub-vertical axial planes and a WNW-ESE orientation associated with a sub-vertical cleavage of crenulation. (Pereira *et al.*, 1993; Noronha *et al.*, 2006).

Post-D3 late phases developed a ductile-brittle and brittle regime, responsible by two conjugates fractures NNE-SSW, with sinistral movement, and NNW-SSE with dextral (Noronha *et al.*, 2006). These fractures control the installation of the post-tectonic Hercynian granites. In that way, different granite types are distributed along alignments coincident in most cases with D3 shear zones (syn- to late-tectonic granites) or along alignments coincident with post-D3 fragile fractures (Ferreira *et al.*, 1987; Noronha *et al.*, 2006).

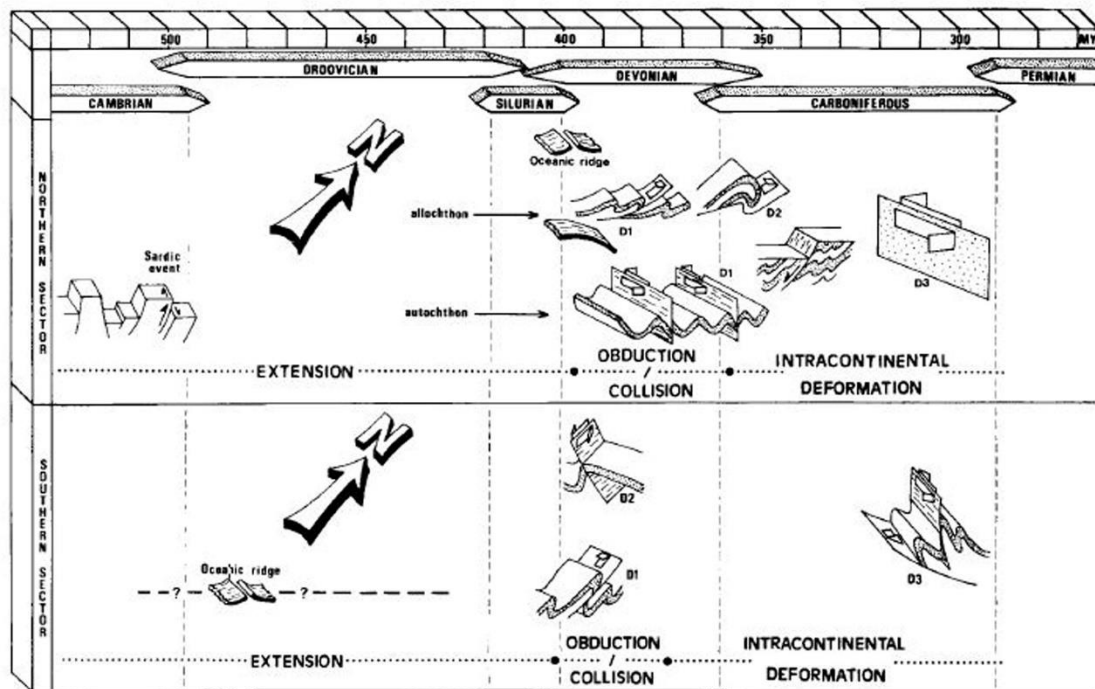


Figure 4 - Main deformation events in the Iberian Peninsula during the Hercynian orogeny (Dias e Ribeiro, 1995).

Hercynian granites can be divided in two groups (Ferreira *et al.*, 1987, Noronha *et al.*, 2006, Dias *et al.*, 2010): two mica granites and biotite granites.

Two mica granites have dominant muscovites and result from crystallization of peraluminous wet magmas from mesocrustal levels by partial fusion of metasedimentary rocks. These granites are syn-tectonic (Sin-D3, 315-310Ma) and are associated with ductile shear zones inside elongated D3 regional antiforms.

The biotitic granites are calc-alkaline rocks and originate in a deep crustal level related with dry magmas. The installation of these granites was conditioned by the shear zones and fractures with N-S and NNE-SSW orientations, and can be from syn- to late-D3, to post-D3.

The Chaves concession lies within Galicia Trás-os-Montes Zone (GTMZ). The GTMZ is related to a nappe emplacement over the CIZ, with two Hercynian deformations phases associated (D1 and D2). This emplacement developed a sub-horizontal foliation (S2). This geotectonic zone is characterized by allochthonous mafic and ultramafic complexes, surrounded by parautochthonous (Ordovician – Lower-Devonian) metasedimentary sequences (Schistose Domain) (Ribeiro, 1974; Mercedes *et al.*, 2011; Doria *et al.*, 2011). The schistose Domain represents a continental margin of Gondwana

whereas the mafic-ultramafic complexes are ophiolitic units with an exotic origin (Perez Estaun et al, 1990; Martinez-Catalan et al. 1996). The Parautochthonous terrane consist in early-Palaeozoic metasedimentary sequences constituted by phyllites, micaschists and quartz greywacke with rare calcosilicated rocks (Ribeiro M. A. *et al.*, 2007). These metasedimentary sequences were intruded by different granitoids.

The installation of post tectonic granites is controlled by the NNW-SSE trending Régua-Verín regional fault, a major shear structure, late-D3, with a polyphasic reactivation. There are other parallel structures, like the Boticas fault cutting this concession area (NNE trending).

### 3.2. Local Geology

The study area is covered by sheets 6-B Chaves and 2-D Vilar de Perdizes, of geological map at scale 1:50.000. The dominant rock type on this area is the two mica granite. This two mica granite intruded in a metasedimentary sequence so called “schist and granite complex” (Figure 5). The two-mica granite vary from medium grained to coarse grained and from equigranular to porphyritic.

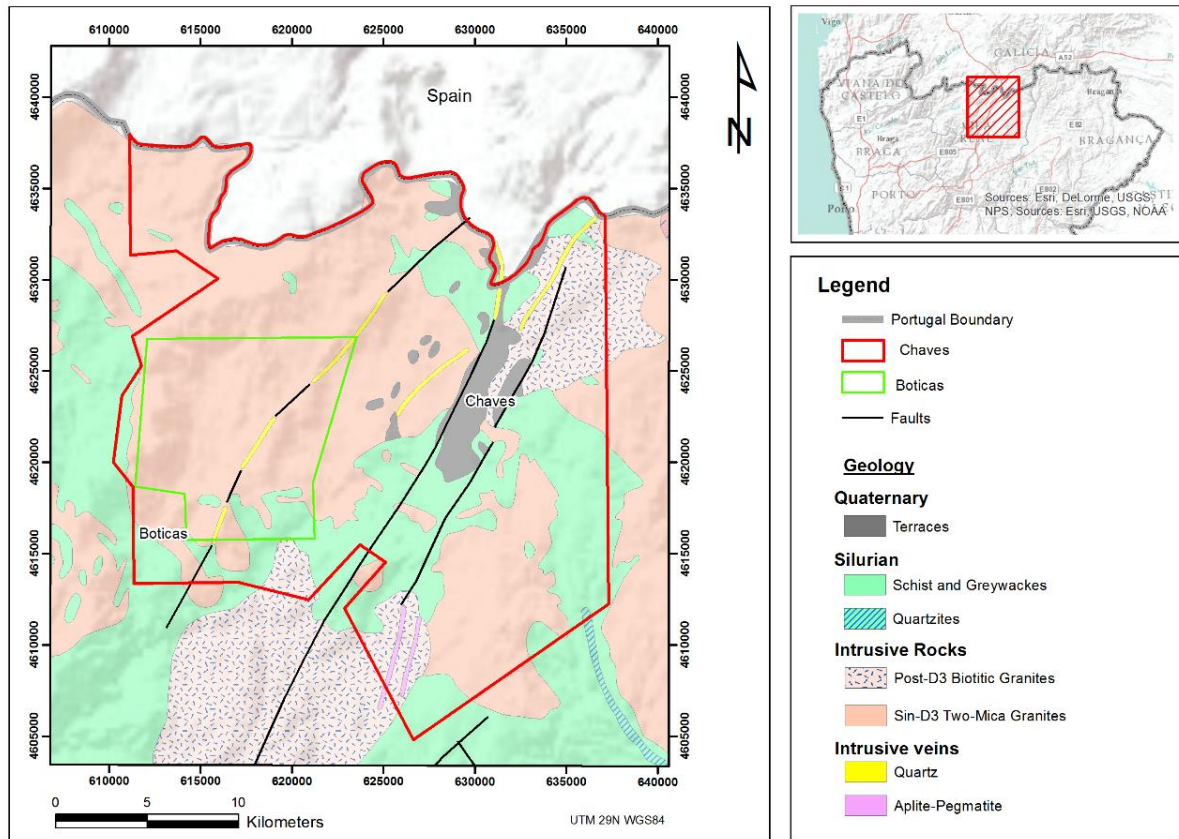


Figure 5 - Geological map of the study area.

The metasedimentary belt is composed by pelitic rocks metamorphosed with intercalations of quartzitic levels, andalusite schists and more rarely graphitic schists.

Two different granites are identified in this concession area. A syn-tectonic two-mica granite is more abundant, with an elongated form NW-SE strike intruded the metasediments and occupies the centre of an antiform striking N130° and formed during D3 phase (Noronha *et al.*, 2013). These granites were affected by late-D3, being fractured and hydrothermally altered. A post-D3 porphyritic biotite granite is less abundant and is associated with Régua-Verín fault and strikes NNE-SSW.

Hydrothermally veined rocks are present, such as quartz veins, aplites and pegmatites. Some alluvium deposits from Plio-Pleistocene can be found along the Chaves valley and some sparse spots.



### 3.3. Gold Mineralization

The gold occurrence in Portugal develops in the septentrional province (Thadeu, 1965). In this province, granite-related deposits with Hercynian age are represented by sub-vertical quartz veins mineralized essentially in arsenopyrite, and minor galena, pyrite, sphalerite and chalcopyrite.

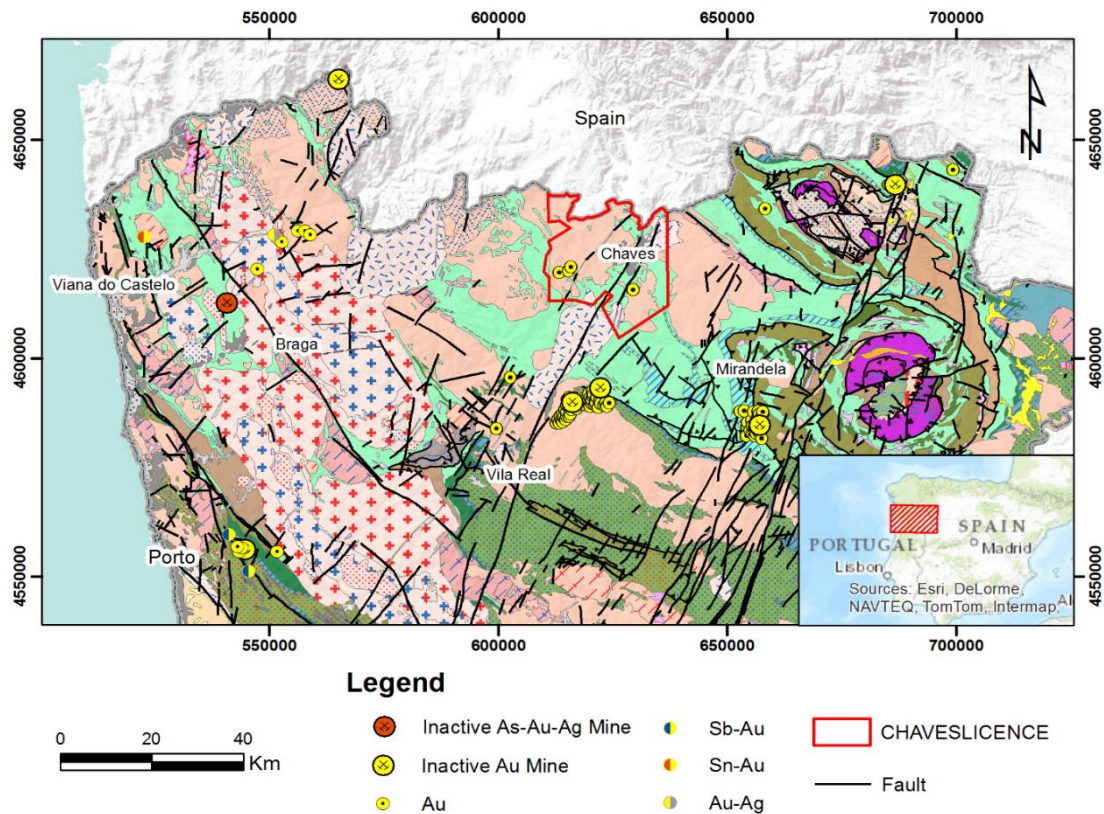


Figure 6 - Gold occurrences in northern Portugal.

Gold occurrences in northern Portugal show a distribution parallel to the Hercynian structures (Figure 6), to the granite massifs and late-Hercynian fractures where veins seem to be affected by different phases of deformation that varied from ductile-brittle to brittle (Noronha & Ramos, 1993; Noronha *et al.*, 2013).

During the orogenic evolution an important fluid production and circulation was responsible for the ore concentration. This concentration was only possible with a slow and constant fluid circuit with different origins along extensive drainage channels. These mineralizing fluids have metamorphic and/or magmatic origin, resultants from rock dehydration that combined with oxidizing meteoric fluids. The main channels responsible for the fluid circulation consist in big crustal discontinuities, developed during ductile-brittle

to brittle regime, where late phases of deformation responsible by fractures NNW-SSE and NNE-SSW have an important role (Noronha, 2000). This fracture system was used for the installation of post-tectonic granites (280-270 Ma) that had an important role as the activator of convective circuits of hydrothermal and meteoric fluids that remobilized the pre-existent gold and concentrate in favourable zones. Gold deposition is related with the progressive dilution and cooling of crustal fluids by the mixture with the meteoric fluids. Gold will deposit in structural and geochemical “traps” and also in microfracturation of sulfides, where gold precipitates by electrochemical process (Noronha, 2000).

Noronha & Ramos (1993) proposed four stages of deposition based on associations of different gold deposits in northern Portugal. The early stage is characterized by the association between oxides and silicates such as rutile, feldspars, cassiterite and wolframite; a later ferric-arsenic stage, characterized by the association of arsenopyrite, pyrite, pyrrhotite and bismuthinite; an intermediary stage of cupriferous zinc, characterized by the association of chalcopyrite and sphalerite and two late stages; a lead-antimoniferous with galena and sulphosalts, and a antimoniferous stage characterized by antimony and berthierite. Based in this mineralogical associations, these authors define three types of occurrences: an association of As-Fe-Bi-Au-Ag-(W-Mo-Sn-Cu-Pb-Zn) corresponding to the mineralogical association of arsenopyrite-pyrite-bismuth-gold-electrum-(tungstate-cassiterite-stannite-molybdenite-chalcopyrite-sphalerite-galena-sulphosalts). Other occurrences of As-Fe-Pb-Zn-Cu-Au-Ag-(Sb-Cd) correspond to a mineralogical association arsenopyrite-pyrite-galena-chalcopyrite-sphalerite-gold-electrum-(sulphosalts); and another characterize by the overlay of the other two associations.

Mercedes *et al.* (2015) made a detailed description of mineralization in the Limarinho deposit, where two gold parageneses were defined. The first, Bi-Te-( $\pm$ S), gold occurs as native, along with native-Bi, hedleyite and joséite-B, in inclusions in sulfides; the second, ( $\pm$ Cu)Ag-Pb-Bi-S $\pm$ Te, gold occur as *electrum* in intergranular spaces, fractures or in cavities of sulfides and quartz gangue, and comprises ( $\pm$ Cu)Ag-Pb-Bi sulfosalts, Pb-Bi sulfotellurides and hessite. In this study, the authors propose two different mechanisms for gold mineralization: a bismuth melt scavenging gold from an Au-unsaturated hydrothermal fluid (Au-Bi-Te $\pm$ S paragenesis); and a gold remobilization together with new gold deposition due to sulfur extraction from the hydrothermal fluid during the stage of prevailing sulfide precipitation. These two events of gold precipitation may have enhanced the gold grade in this deposit.

### 3.3.1. Local Gold Mineralization

The known mineralization in the study area occur in syn-tectonic two mica granites, in quartz veins or veinlets, sometimes in stockwork, in centimetric massive sulfides and sometimes disseminated in granite. Mineralized quartz veins have a strike N20° - 40°, subvertical dip, with a thickness between 2 cm up to 20 cm. These gold-bearing quartz veins run almost parallel to the major Régua-Verín fault and their emplacement is structurally controlled. Thicker quartz veins (up to 3 meters thick) are visible but they are sterile in gold.

This mineralization is late- to post-tectonic and occurs at depth in mesothermal to epithermal conditions resulting from the circulation of metamorphic fluids and meteoric fluids that result in precipitation of quartz, arsenopyrite, pyrite, gold and sulphosalts, mostly tellurides and bismuthides (Harford *et al.*, 1998; Mendonça, 2006).

A strong correlation between gold grade and arsenopyrite content has found. The higher gold contents are associated with arsenopyrite-rich material, however, not all arsenopyrite rich material have high gold grades.

The areas with a great vein density are accompanied by a strong alteration in the wall rocks. This process of hydrothermal alteration is related with the interaction between wall rocks and hydrothermal fluids that include heat and chemical constituents inducing wall rock compositional variations. Hydrothermal alteration provides a significant guide to mineral exploration, although the presence of alteration does not necessarily guarantee the occurrence of gold mineralization.

### 3.3.2. Structural Control of gold mineralization

The Régua-Verín fault has an important role in this region, playing a strong control on gold mineralization. Several deposits occur along this structure such as Jales and Tresminas, etc. (Claverol *et al.*, 1987; COGEMA, 1990; Mendonça, 2006). This major fault also have a strong control in the study area, where the mineralizations demonstrate a subparallel direction to this structure.

Griveaud and Dixsaut (1989) made a detailed structural analysis for known mineralized zones (Limarinho, Poço das Freitas and Batocas) and demonstrated that gold bearing veins are dominant in a NE trend. An N-trending subordinate group was identified but are minimally mineralized. The authors proposed a stress field rotation (Figure 7 and 8) occurred during the mineralizing event, with initially N-trending sinistral strike-slip producing one auriferous veins set, and then a rotation of the sinistral strike-slip direction to a NE orientation producing cross-cutting veins and faults. Another subsidiary grouping in the sub-horizontal sector but with dominant N strike was attributed to shallow dipping foliation and pegmatite intrusion in the granite (COGEMA, 1990; Harford *et al.*, 1998)

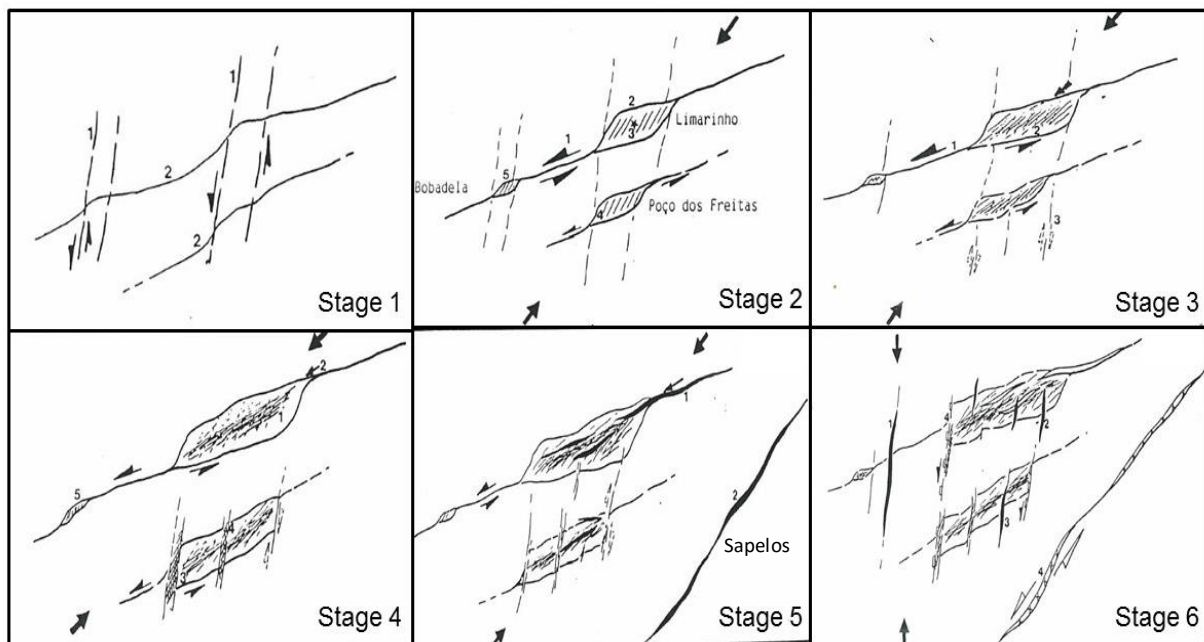


Figure 7 – Structural evolution of Bobadela, Limarinho and Poço das Freitas sector. (Adapted from Griveaud and Dixsaut (1989). Stage 1 – N-S shear zones with left movement affect N60° shear zones. Stage 2 and stage 3 – N60° sinistral shears created an extensional zone at the intersection of the two strike-slip faults. These extensional zones acted as a conduit for the fluids, forming quartz veins which followed the formation of hydraulic breccia mineralized with hematite. Occurred the installation of N30-N40° quartz veins with arsenopyrite. Stage 4 – Intensification of the movement result in a denser parallel network of mineralized veins in the center of dilation zones. Stage 5 – End of mineralizing fluids. Emplacement of milky quartz veins, sterile or weakly mineralized, with N60° trend at Limarinho and Sapelos. Stage 6 – Changing in the shortening direction, from N60° to N-S, resulting in new openings with infillings of white quartz. Normal and/or sinistral movement in N-S TO N20° faults at south of Limarinho caused offset of mineralized structures at Poço das Freitas. Sinistral movement of the Sapelos fault caused brecciation of the vein.

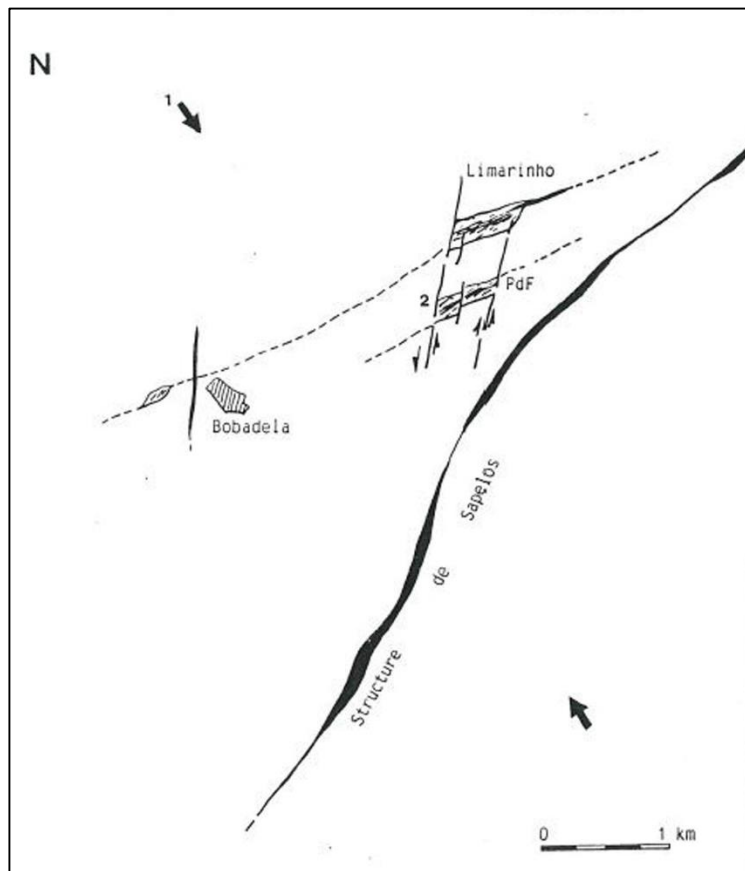


Figure 8 – Actual structural stage of Bobadela, Limarinho and Poço das Freitas sector. (Adapted from Griveaud and Dixsaut (1989). Late brittle stage with the shortening direction N140°E (1), allowing the sinistral movement in the N-S faults (2) which accentuates the offset of mineralized structures.

### 3.4. Fluid chemistry & P-T conditions

Noronha et al. (2013) describe the P-T conditions of gold bearing quartz vein for this region based on earlier studies that describe fluid inclusions present in milky quartz, as a thermic metamorphism, syn-D3, with an intermediate temperature ( $300^{\circ}\text{C} < T < 500^{\circ}\text{C}$ ) and a low pressure ( $P \sim 300\text{-}400\text{MPa}$ ). The progressive  $\text{CH}_4$  and  $\text{H}_2\text{O}$  enrichment and density diminution of volatile phase are interpreted as a consequence of a progressive dilution by an aqueous component. The circulation of these fluids, occurred along shear zones, syn- to late-D3 with a  $P < 200\text{MPa}$  and a  $350^{\circ}\text{C} < T < 300^{\circ}\text{C}$ .

Gold deposition occurred later with a  $P < 100\text{ MPa}$  and  $T < 300^{\circ}\text{C}$ . These conditions are indicative of an uplift after the D3 phase (Boiron *et al.*, 1996; Noronha *et al.*, 2000; Noronha *et al.*, 2013)

Deposition of gold is related with late fluids, dominantly aqueous with low salinity with a P and T indicatives of a depth around 2 Km (Noronha *et al.*, 2013)

Doria *et al.* (2011) in a fluid inclusion study of gold bearing arsenopyrite-rich quartz vein system describes the fluids involved in the mineralizing process. It was recognized three types of fluids by petrographic, micro-Raman and Microthermometric studies:

- I. Aqueous-carbonic  $\text{H}_2\text{O}-\text{CO}_2-\text{CH}_4-\text{N}_2-\text{NaCl}$
- II. Aqueous with low to medium salinity  $\text{H}_2\text{O}-\text{NaCl}$
- III. Aqueous with high salinity  $\text{H}_2\text{O}-\text{CaCl}_2-\text{NaCl}$

They conclude that an evolution of aqueous-carbonic fluids occurred and is probably related to the earlier sulfides, to late aqueous fluid with low to medium salinity and finally to high salinity fluids. These fluids display similar features to those found in Hercynian gold mineralizations from the Iberia (Noronha *et al.*, 2000).

Mercedes *et al.* (2015) in a study of the Au-bearing vein system of the Limarinho deposit defined two main stages of mineral deposition for quartz veins (stage I and II), with successive period of vein re-opening, and are crosscut by irregular veinlets (stage III). The first two stages (I and II) correspond to an As-Fe mineralization, where arsenopyrite and quartz are the more abundant minerals; the final stage II and stage III are characterized by a Pb-(Zn)-Fe-Cu sulfides and chlorite. In this study they defined the hydrothermal fluids in stages I and II as low salinity aqueous-carbonic, increasing the  $\text{CH}_4 + \text{N}_2$  amount toward the stage II, indicating mixing with metamorphic fluids; it was inferred for stage I temperatures of  $460 \pm 40^\circ\text{C}$  and pressures from 230 to 350 MPa and for the stage II was estimated temperatures from 340 to  $425^\circ\text{C}$  and pressures from 60 to 225MPa. This means that occur a decompression of more than 250MPa between these two stages. Late stage II and stage III are related to aqueous fluid with variable salinity as result of mixing between a hotter and saline fluid with a cooler and dilute, probably with meteoric origin. Temperatures from  $300^\circ\text{C}$  to lower than  $200^\circ\text{C}$  and pressures around 60MPa, for stage III were defined.

## 4. Data & Image Processing Methods

### 4.1. Data

#### 4.1.1. Geological Data

The geological data used in this study was obtained from different sources as: Geological Map of Portugal with scale 1:50.000 6-B Chaves (Teixeira and Medeiros, 1969), Geological Map of Portugal 1:200.000, sheet nº2 (Pereira *et al.*, 2001), structural data from COGEMA and Medgold databases, geochemistry data from Minas Romanas (BLEG study), etc.

Some of this geological data was digitalized and georeferenced using WGS 84 Datum, UTM 29N, in order to use in the GIS software.

#### 4.1.2. Landsat data

The Landsat program consists in a continuous acquisition of space-based moderate resolution land remote sensing data (USGS, 2015d, 2015e). Since 1972, seven Landsat missions were completed that acquired imagery used in several research areas, such as geology, agriculture, forestry, mapping, regional planning, etc. This Landsat project consists in a collaboration between the National Aeronautics and Space Administration (NASA) and the USGS, ensuring the continuous acquisition and data availability (Sabins, 1999; Powell 2007; Markham, 2012; USGS, 2015a).

Table 3 summarizes the history of the Landsat series of satellites (NASA, 2011). Over the years, Landsat enhanced the number of spectral bands and spatial resolution.

Table 3 - Landsat systems, operational dates and sensors. In Markham 2012.

Landsat satellite	Launch	Decommissioned	Sensors	
Landsat-1	July 23, 1972	January 6, 1978	MSS (4 bands)	RBV (3 bands)
Landsat-2	January 22, 1975	February 5, 1982	MSS (4 bands)	RBV (3 bands)
Landsat-3	March 5, 1978	March 31, 1983	MSS (5 bands)	RBV (pan only)
Landsat-4	July 16, 1982	June, 2001	(TM (7 bands)	MSS (4 bands)
Landsat-5	March 1, 1984	2013	TM (7 bands)	MSS (4 bands)
Landsat-6	October 5, 1993	Failed to achieve orbit	ETM (8 bands)	
Landsat-7	April 15, 1999	Operational	ETM+ (8 bands)	
Landsat-8	February 11, 2013	Operational	OLI (9 bands)	TIRS (2 bands)

These four Landsat instruments generations (MSS, TM, ETM+ and OLI (and TIRS) have different band designations. Landsat Multispectral Scanner (MSS) imagery consist in four spectral bands with 60 meter spatial resolution. Each image covers approximately an area of 170 km (north-south) by 185 km (east-west). Specific band designations differ from Landsat 1-3 to Landsat 4-5 (USGS, 2015d).

Landsat Thematic Mapper (TM) images are composed by seven spectral bands with a spatial resolution of 30 meters for Bands 1 to 5 and 7 and for Band 6 (thermal infrared) is 120 meters, but is resampled to 30-meter pixels. Approximate scene size is 170 km (north-south) by 183 km (east-west) (USGS, 2015d).

Landsat Enhanced Thematic Mapper Plus (ETM+) imagery consists of eight spectral bands with a spatial resolution of 30 meters for Bands 1 to 7 and the Band 8 (panchromatic) resolution is 15 meters. Scene size is approximately 170 km (north-south) by 183 km (east-west) (USGS, 2015d).

On May, 2013 Landsat 8 Operational Land Imager (OLI) became available as well as Thermal Infrared Sensor (TIRS) imagery. This data consists of nine spectral bands (Table 4) with a spatial resolution of 30 meters for Bands 1 to 7 and 9, and 15 meters resolution for Band 8 (panchromatic). New band 1 (ultra-blue) is useful for coastal and aerosol studies and new band 9 is useful for cirrus cloud detection. Bands 2-4 are visible bands whereas band 5 corresponds to near infrared (NIR). In addition, Band 6 and 7



correspond to shortwave infrared (SWIR) spectrum. Thermal bands 10 and 11 are useful in providing more accurate surface temperatures and are collected at 100 meters resolution. Approximate capture scene size is 170 km (north-south) by 183 km (east-west).

Table 4 – OLI and TIRS bands characteristics. (USGS, 2015a).

<b>Landsat 8 Operational Land Imager (OLI) and Thermal Infrared Sensor (TIRS)</b>		
<b>Bands</b>	<b>Wavelength (micrometers)</b>	<b>Ground Sampling Distance (meter per pixel)</b>
Band 1 – Coastal aerosol	0.43 - 0.45	30
Band 2 – Blue	0.45 - 0.51	30
Band 3 – Green	0.53 - 0.59	30
Band 4 – visible Red	0.64 - 0.67	30
Band 5 – Near Infrared (NIR)	0.85 - 0.88	30
Band 6 – SWIR 1	1.57 - 1.65	30
Band 7 – SWIR 2	2.11 - 2.29	30
Band 8 – Panchromatic	0.50 - 0.68	15
Band 9 – Cirrus	1.36 - 1.38	30
Band 10 – Thermal Infrared (TIRS) 1	10.60 - 11.19	100 * (30)
Band 11 – Thermal Infrared (TIRS) 2	11.50 - 12.51	100 * (30)

\* TIRS bands are acquired at 100 meter resolution, but are resampled to 30 meter in delivered data product.

For this study, Landsat 8 OLI multispectral imagery was used (path 204; row 31) acquired on May 9, 2015 under excellent weather conditions (1.24% cloud cover) and excellent image quality. The image package consists in a 11 band images (GeoTIFF), 1 quality assessment band image ( GeoTIFF) and 1 metadata file (ASCII). This imagery was obtained from Earth Explorer (USGS, 2015f), a search interface with access to USGS archives, where it's possible free download different data products, as Landsat data. The image map projection is UTM zone 29N (WGS84 datum). Gathering data in visible, SWIR regions have a particular interest for geological application (Rajesh, 2004; Mwaniki *et al.*, 2015; USGS, 2015a, b):

- Band 7 (SWIR: 2.11-2.29  $\mu\text{m}$ ) – Coincides with absorption band caused by hydrous minerals (clay mica, some oxides, and sulfates) making them appear darker. Normally used in lithological mapping
- Band 6 (SWIR: 1.57-1.65  $\mu\text{m}$ ) – soil and rock discrimination: this band is sensitive to moisture variation in vegetation and soils; it is sensitive to presence of ferric iron or hematite rocks.
- Band 4 (Visible: 0.64-0.67 $\mu\text{m}$ ) – discrimination of soil from vegetation: This band is good for discriminating soil and vegetation and delineating soil cover.

### 4.1.3. GIS Software

GIS software was used for preprocessing, enhancement, to classify remote sense imagery and to extract spatial information. This is an effective tool for integration and for analysis of large amount of georeferenced spatial data with different formats and attributes. ArcMap 10.2 from ESRI and QGIS 2.8.2 were the GIS software used (commercial software and open source software, respectively). Rajesh (2004) defines four steps to map mineral potential occurrence areas using GIS:

- Build a database containing spatial digital data;
- Extract predictive evidence for a particular mineral deposit type;
- Calculate weights for each predictive evidence map;
- Combine the maps to predict mineral potential.

The data collected (geochemical data, geological data (lithology and structural), satellite data, topographical data (DEM), mineral occurrence data and ground survey data) used in this study were spatial analyzed in way to generate a final target exploration map.

## 4.2. Image Processing

### 4.2.1. Pre-processing

As already stated, for mineral exploration mapping, the most appropriated bands are located in the visible, NIR and SWIR regions. In this work, bands 2 to 7 from Landsat 8 OLI and the panchromatic (band 8) were used. This panchromatic band has a higher spatial resolution when compared with the multispectral bands, and was used as a sharpening band or as a greyscale base image. The raw images were quantized and calibrated scaled Digital Numbers (DN). The Landsat imagery are currently corrected by USGS EROS Center, with radiometric correction for accurate measurements at the sensor and no data loss, and geometric correction with ground control and corresponding Digital Elevation Model points from accurate ground location (USGS, 2015a).

This data was converted to the Top of Atmosphere (TOA) reflectance using radiometric coefficients (USGS, 2015b), where DN are converted to reflectance representing the ratio of the radiation reflected off a surface to the radiation striking it (Han and Nelson, 2015). The following equation was used to convert DN values to TOA reflectance:

Where:

$$\rho_{\lambda} = \frac{M_{\rho} * Q_{cal} + A_{\rho}}{\sin(\theta)}$$

$\rho_{\lambda}$  = Top-of-Atmosphere Planetary Reflectance (unitless).

$M_{\rho}$  = Reflectance multiplicative scaling factor for the band.

$A_{\rho}$  = Reflectance additive scaling factor for the band.

$Q_{cal}$  = Level 1 pixel value in DN.

$\theta$  = Solar Elevation Angle

Usually, image enhancement is required for a better interpretation of the study area. This operation consists in a stretch imagery contrast to improve the information content of the image. Spatial filtering techniques provides better visualization, highlighting or suppressing some features of the image that allows to extract oriented features. These filters works based on spatial frequency, so rapid variations in brightness

levels can indicate roughness and low spatial frequency smoother areas (Rajesh, 2004; Hung *et al.*, 2005; Sukumar *et al.*, 2014).

## 4.2.2. Image Processing Methods

Image processing methods transform the multispectral satellite data into images that enhance geological features in contrast with the background. In this study, enhancements techniques, such as Band composite, Band Ratioing and Principal Component Analysis (PCA) were applied which allowed the extraction of spatial and spectral information related to lithology, structures, hydrothermal alteration, and others. These techniques allow to create a mineral potential map of gold mineralization occurrence and delineate mineral exploration targets for further work. Target delineation involves the analysis and integration of various thematic geological data. To achieve the predictive map, data driven (empirical) and knowledge driven (conceptual) methods were applied for conjugation of the different geo-spatial data, where the results were conditioned by structural, lithological and geochemical controls. (Bonham-Carter, 1994; Moradi *et al.*, 2015)

### 4.2.2.1. Single Band Combinations

Landsat imagery is composed by grey-scale images correspondents to spectral bands. When a composite of three bands (red, green, and blue) is created a colourful multispectral image will result, which can be true colour or false colour (in this case, a NIR band is used instead of blue band). There are different band combinations possibilities whereby some of them enhance relevant features for mineral exploration.

A composite with the visible bands of the spectrum, that correspond to red, green and blue, is called a true colour composite. When a composite is created with non-visible bands it is called a false colour composite image. In a false colour image, the combination of three bands (visible bands and infrared bands or only infrared bands) in red, green and blue will produce an image that enhance some characteristics depending the selected spectral bands. The bands are assigned based on spectral properties of the rocks and alteration minerals.

Some band composites are useful in a first approach for mineral and rock discrimination and interpret possible alterations based in colour intensity variations, as RGB (7, 5, 2) or the RGB (5,6, 7).

#### 4.2.2.2 Band Ratio

Band ratioing is a technique where digital numbers (brightness values) of one band are divided by that of another band. This corresponds to the peaks of high and low reflectance curve (Vincent and Thompson, 1972; Goetz *et al.*, 1975, Pour *et al.*, 2015). This technique improve the contrast and enhances compositional information while suppressing useless information, like earth's surface and shadowing caused by topography surface shadow, allowing highlight some features that cannot be seen in raw data (Sabins, 1997; Rajesh, 2004; Van der Meer, 2012; Ali & Pour 2014).

Different band ratios were tested in this work, in order to enhancing hydrothermally altered rocks and lithological units. The selection of bands are related to the spectral reflectance and position of the absorption bands of the mineral or assemblage of minerals to be mapped. Some authors refer the following band ratios for geological use, usually used to enhance lithological features (Sabins, 1999; Rajesh, 2004; Zoheir *et al.*, 2012; Han and Nelson, 2015; Mwaniki *et al.*, 2015):

- 4/2 – iron oxide
- 6/7 – hydroxyl bearing rock
- 7/5 – clay minerals
- 6/5 – ferrous mineral

Minerals such as alunite, and clay minerals such as illite, kaolinite and montmorillonite have distinctive absorption (low reflectance) features as ~2200nm and low absorption at ~1600 nm (Figure 9) (Sabins,1999); iron oxides and sulphate minerals commonly have a strong reflectance near red and low blue reflectance (Figure 9) (Hans and Nelson, 2015). The ratio of Landsat 8 band 6 (1570 nm – 1650 nm) over band 7 (2110 – 2290) can be applied to distinguishes altered rocks containing clays and alunite from unaltered rocks. Areas with abundant iron minerals are shown with the ratio image of Landsat 8 OLI band 4 (640-670 nm) over band 2 (450-510 nm). (Sabins, 1999; van der Meer *et al.*, 2012; Han and Nelson, 2015).

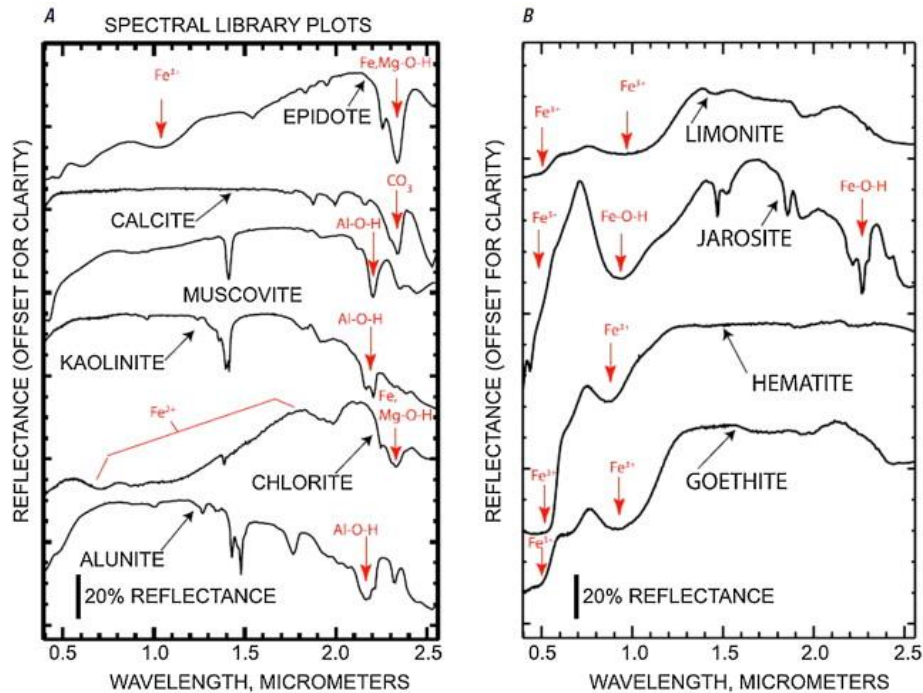


Figure 9 – (A) Laboratory spectra of alunite, chlorite, kaolinite, muscovite, calcite, and epidote. (B) Laboratory spectra of limonite, jarosite, hematite and goethite (Clark et al., 1993).

When using colour composites, the bands are selected based on spectral reflectance and the absorption features of the minerals or mineral assemblage to be mapped. An image incorporating these band ratios will discriminate altered from unaltered ground and highlight areas where concentration of these minerals occurs (Rajesh, 2004). Ali and Pour (2014) refers the Sabin's ratio (4/2, 6/7 and 6/5 as RGB) for lithological mapping and hydrothermal alteration zones. The ratio 4/2 is used for mapping iron oxides as hematite, limonite and jarosite, and has high reflectance in red region (Van der Meer, 2004). The ratio 6/7 is used to map clay minerals as kaolinite, illite and montmorillonite. The ratio 6/5 will show high reflectance in presence of ferrous minerals.

Pour et al. (2015) refer to a band ratio for identification of hydrothermal alteration minerals. The RGB image (4/2, 6/7, 5) was created to allow the identification of lithology, altered rocks and vegetation. With the same purpose, Kaufmann ratio (7/5; 5/4; 6/7) was also used (Ali and Pour, 2014).

### 4.2.2.3 Principal Components Analysis (PCA)

The Principal Components Analysis (PCA) is a technique used to enhance and separate certain spectral signatures from the background (Gabr *et al.*, 2010, Moradi 2015). PCA consists of a linear transformation applied on highly correlated multidimensional data like multispectral imagery which has a similar visual appearance for different bands, causing data redundancy (high correlation of spectral bands) (Loughlin, 1991). Thus, PCA analysis consists of a multivariate statistical technique that selects uncorrelated linear combinations (eigenvector loadings) of variables in such a way that each successively extracted linear combination, or Principal Component (PC) has a lower variance (Singh and Harrison, 1985; Bodruddoza Mia and Fujimitsu, 2012). The number of output PCs is the same as the number of the input spectral bands.

The first Principal Component, PC1, contains most of the data variability, and highlights features common to all input bands and often display important structural info. PC1 corresponds to a vector in the direction of the maximum variance of pixels in the scene. The second PC, PC2, contains the second most data variability. It is orthogonal to PC1 in  $n$  directional space and highlights the spectral differences between visible and the infrared spectral bands. Third PC, PC3 includes the third most variability and is orthogonal to the other two PCs. The other PCs have less variability (Vincent, 1997, Gabr *et al.*, 2010; Moradi, 2015).

The PCs analysis can be used in a standard or selective method (Rajesh, 2004; Van der Meer, 2012). In a standard analysis, all the available spectral bands are used in the input for the PC calculation; in a selective analysis a PCA at selected input bands was applied. For enhancement of hydrothermal alteration zones, the bands with spectral characteristics of the dominant altered minerals in visible, NIR and SWIR regions of spectrum were selected.

The feature-oriented PCs method (Loughlin, 1991) was used in this study in order to enhance iron oxide and hydroxyl bearing areas. In this selective method, bands with spectral signatures for iron and hydroxyl bearing minerals was only used (Crosta and Rabelo, 1993; Rajesh, 2004; Van der Meer *et al.*, 2012). Iron oxides are a constituent of alteration zones associated with hydrothermal sulfide deposits and can be highlighted by band 4 / band 2 ratio (Sabins, 1999; Poormirzaee and Oskouei, 2010, Pour and Hashim, 2015). Hydroxyl bearing minerals are the most widespread product of alteration and correspond to a diversity of clays and sheet silicates, which contain Al-OH and Mg-

OH bearing minerals and hydroxides in alteration zones (Poormirzaee and Oskouei, 2010). The band ratio 6/7 will highlight areas of altered zones comprising dominantly hydroxyl-bearing minerals (Sabins, 1999).



## 5. Results and Interpretations

In this chapter, the results that were obtained from remote sensing imagery processing techniques of the study area are presented. These results were analysed, compared and combined with the geological data. The combination of the extracted information allowed define new targets, possibly associated with gold occurrences in this concession area.

### 5.1. Image Analysis

#### 5.1.1. Single Band Combinations

Single band combinations were applied in a first approach, in order to analyze the study area and visually interpret the multispectral imagery. Using Landsat 8 OLI imagery, six bands (B2, B3, B4, B5, B6 and B7) were available to produce different band combinations, some of them enhancing relevant features for mineral exploration. A true colour image was produced with Landsat 8 visible bands 4, 3 and 2 (Red, Green and Blue, respectively) (Figure 10). With this band combination, it's possible to do an exploratory analysis of the area, identifying rock exposure areas (brown), vegetated areas (green), rivers and lakes (blue) and urbanized areas. In addition, some structural features such as faults and fractures can be identified.

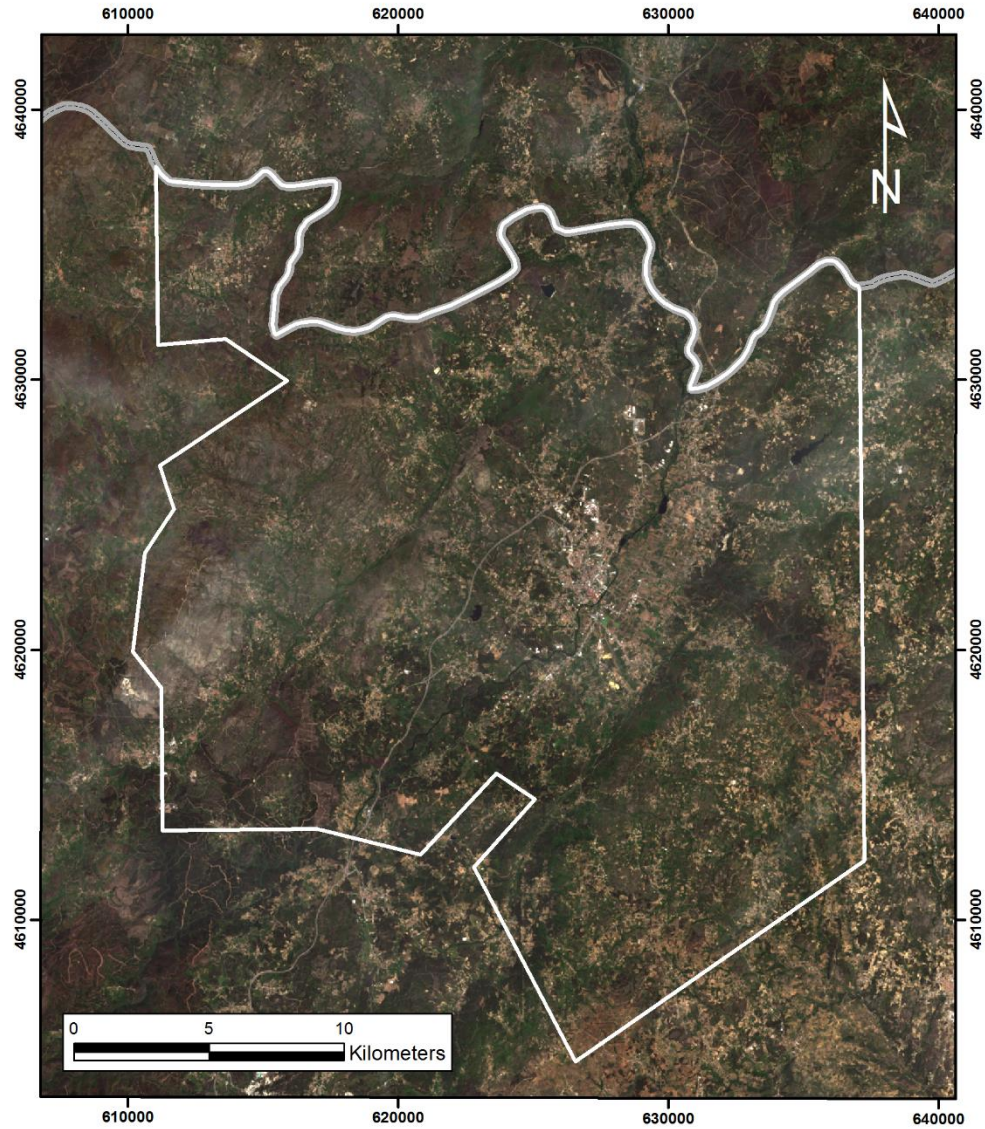


Figure 10 - True Colour image. RGB combination of bands 4, 3, 2. Green colour represent vegetation, brown and brown represent soil or rock and blue water.

A False Colour image was created, using bands 5, 4 and 3 (R, G, B) (Figure 11). This band combination allows a better differentiation between vegetated areas (red areas) and good exposure outcrops (greyish colours). Light blue colour represent urbanized areas.

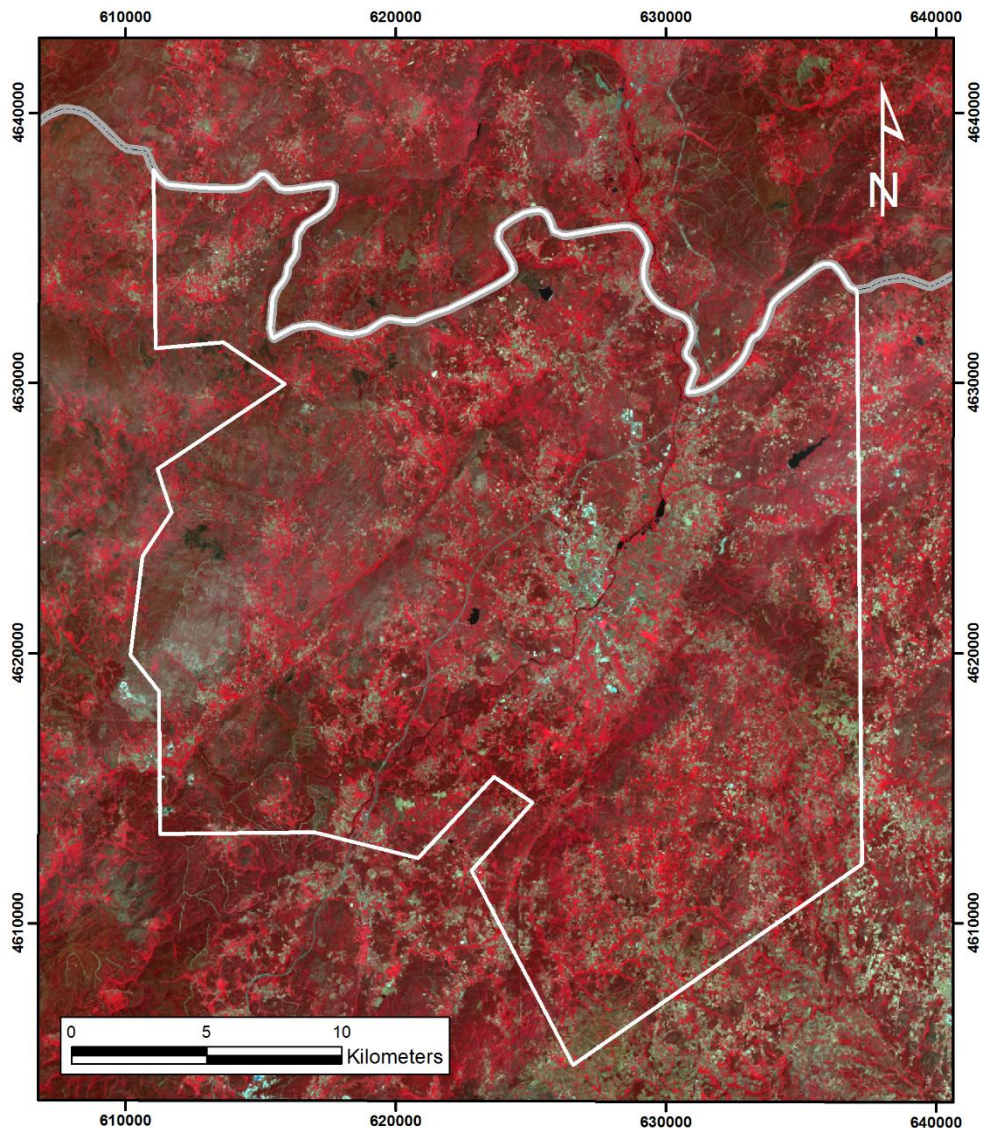


Figure 11 – False Colour Composite. RGB combination of bands 5, 4, 3. Red colour represent vegetation, black represent water and rock or soil are represented by greyish colour. This RGB combination highlights the boundaries between vegetated and outcrop areas.

For a preliminary geological study, a contrast-enhanced RGB combination (SWIR, NIR, and Visible) was created. The most contrasting band combination for lithological features and that provide more detail without additional enhancement should include one visible (2, 3 and 4), one NIR (5) and one SWIR (6 or 7) band (USGS, 2015a; USGS, 2015c). Based on this assumption, a composite using the bands 7, 5, 2 (RGB) was created (Figure 12) where it's possible identify outcrops as shades of orange and red, vegetation in light green and water in black.

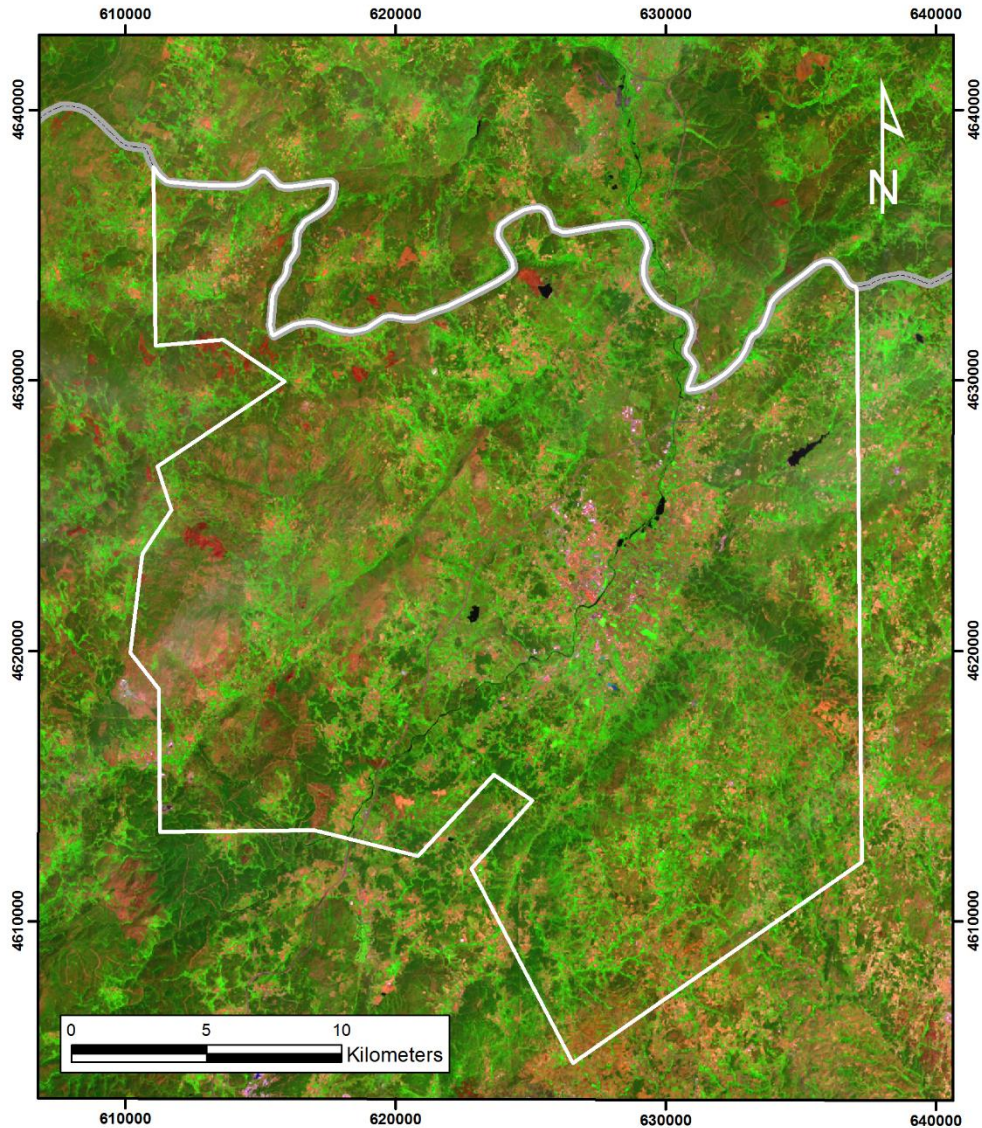


Figure 12 - RGB combination for bands 7, 5, 2. Enhanced image where outcrops are represented in shades of orange and red, Vegetation in light green and water in black.

A band combination with a NIR band (band 5) and two SWIR bands (band 6 and band 7) was created, allowing a regional scale detection of geological features like faults, and differentiation of rock outcrops from vegetation (Figure 13). In this image, rock outcrops show a light blue colour, while vegetated areas an orange colour and water a black. Some hydrothermal alteration in outcrops areas can be identified as blue.

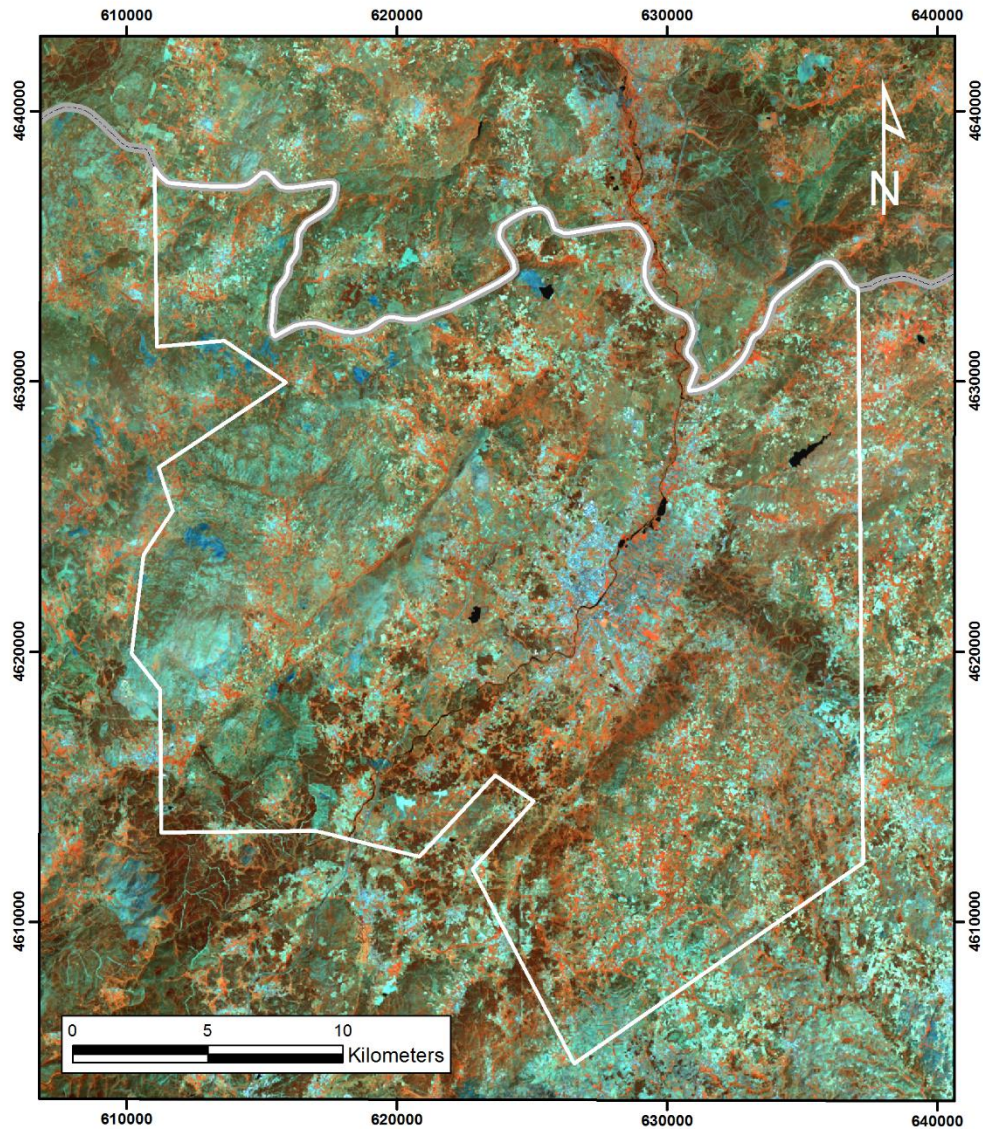


Figure 13 – RGB combination for bands 5, 6, 7. In this image vegetated areas appear in orange colour, outcrops in light blue and water in black. Some hydrothermal altered rocks can be identified as blue.

### 5.1.2. Band Ratio

Images enhancing hydrothermal altered rocks using band ratios with distinctive reflection features were produced. This corresponds directly to minerals associated with this alteration and represents surface expression for auriferous deposits. Thus, it was applied the ratio of Landsat 8 OLI band 4 over band 2, to highlight areas with abundant iron oxides bearing minerals, as brighter pixels (Figure 14 (a)). Ratio of Band 6 over band 5 discriminate ferrous minerals in bright tone (Figure 14 (b)). Clay minerals, as illite, kaolinite, and montmorillonite are discriminated with the ratio image of band 7 over band 5 as bright pixels (Figure 14 (c)). The ratio image of band 6 over band 7 distinguish

altered rocks containing clays and alunite from unaltered rocks, where pixels are bright (Figure 14 (d)).

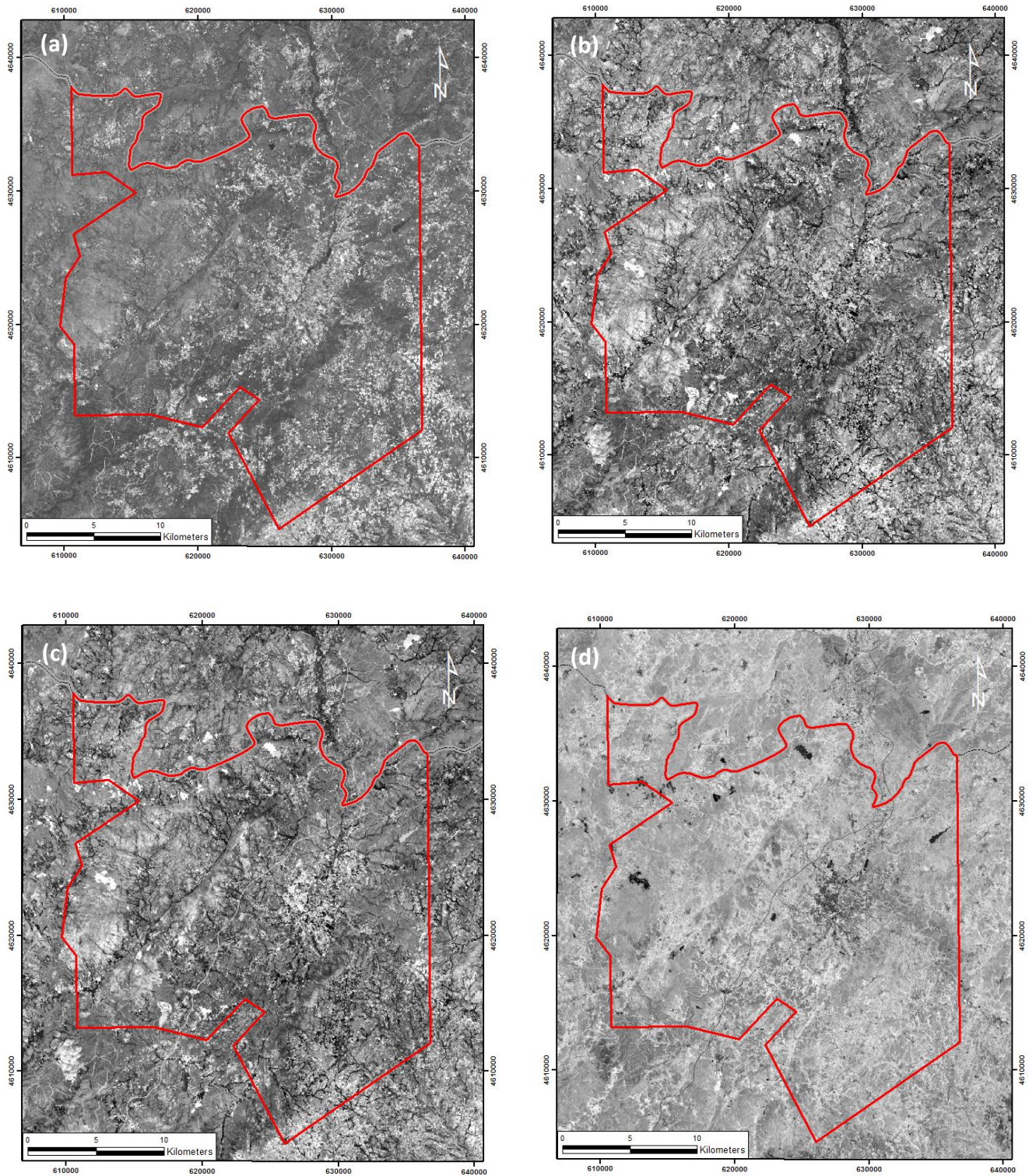


Figure 14 – (a) Landsat 8 band ratio 4/2 image reveals areas where iron minerals (hematite, goethite, limonite, etc.) are abundant shown in bright tones; (b) Landsat 8 band ratio 6/5 image discriminates ferrous minerals with bright tone. (c) Landsat 8 band ratio (7/5) image reveals clay minerals, as illite, kaolinite and montmorillonite, in bright tones. (d) Landsat 8 band ratio 6/7 image shows alunite and hydrothermal clay minerals in bright tones.

An image incorporating these band ratios will discriminate altered from unaltered outcrop and highlight areas where concentration of these minerals occurs. An image using Sabin's ratio (4/2, 6/7 and 6/5 as RGB) was produced for lithological mapping and hydrothermal alteration zones (Figure 15). The ratio 4/2 was used for mapping iron oxides as hematite, limonite and jarosite, and has high reflectance in red region. The ratio 6/7 it's used to map clay minerals as kaolinite, illite and montmorillonite. The ratio 6/5 shows high reflectance in presence of ferrous minerals. In this Figure 15, light blue-yellow colour represent outcrops and blue areas represent vegetation. Light green areas highlights hydrothermal alteration in outcrop rocks.

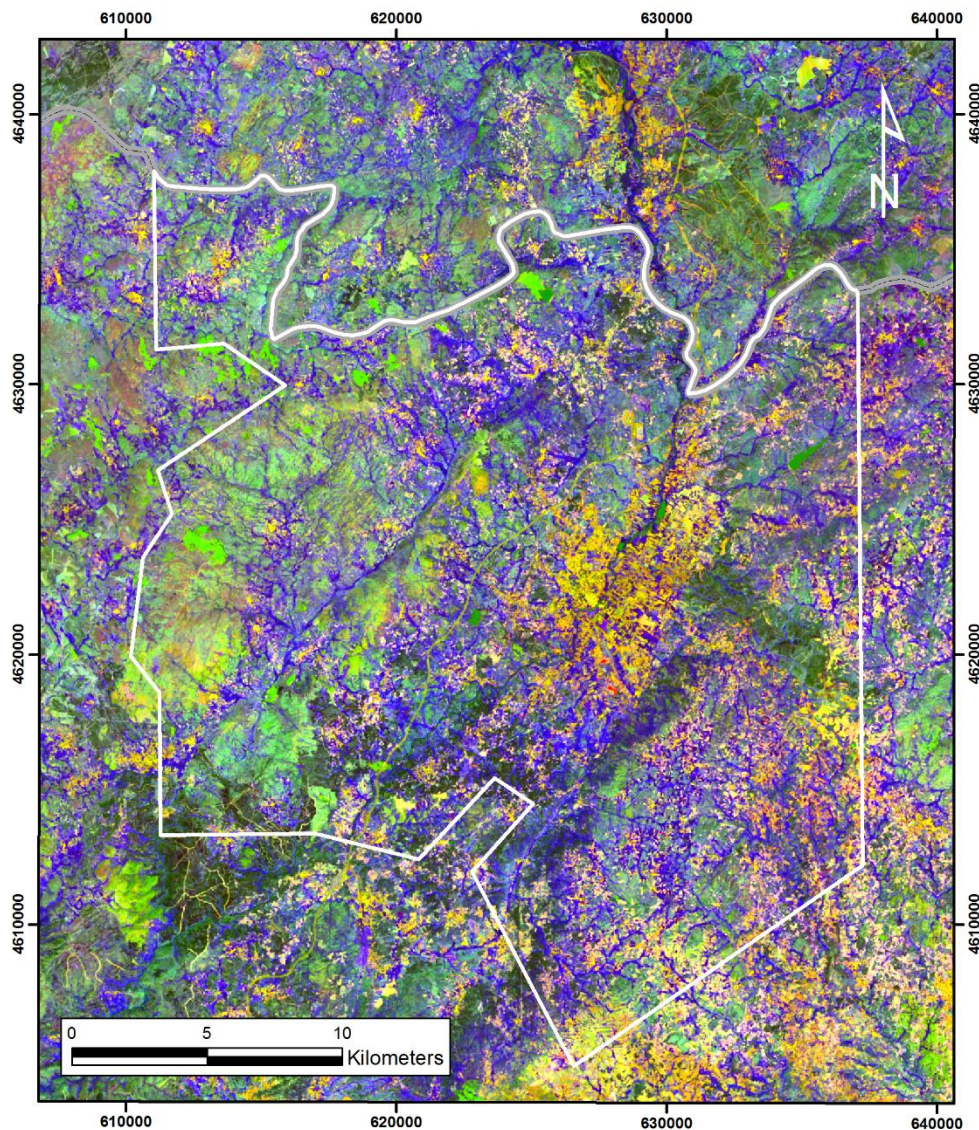


Figure 15 - Sabin's ratio image (4/2, 6/7, 6/5). Outcrops are represented in light blue-yellow colour, vegetation in blue and water in dark green. Strong yellow represent buildings and other human constructions and light green altered rocks.

An additional RGB composite was created with bands 4/2, 6/7, 5, and allows the identification of outcrops as rose and light brown, altered rocks as red areas and vegetation in light blue (Figure 16). Also, other band ratio composite, Kaufmann ratio (7/5; 5/4; 6/7) was tested (Figure 17), that revealed as a good combination for geological purposes. In this image (Figure 17), rose areas represent granite outcrops, metasediments are highlighted as dark green and light blue represent vegetation. Hydrothermally altered rocks are identified as red.

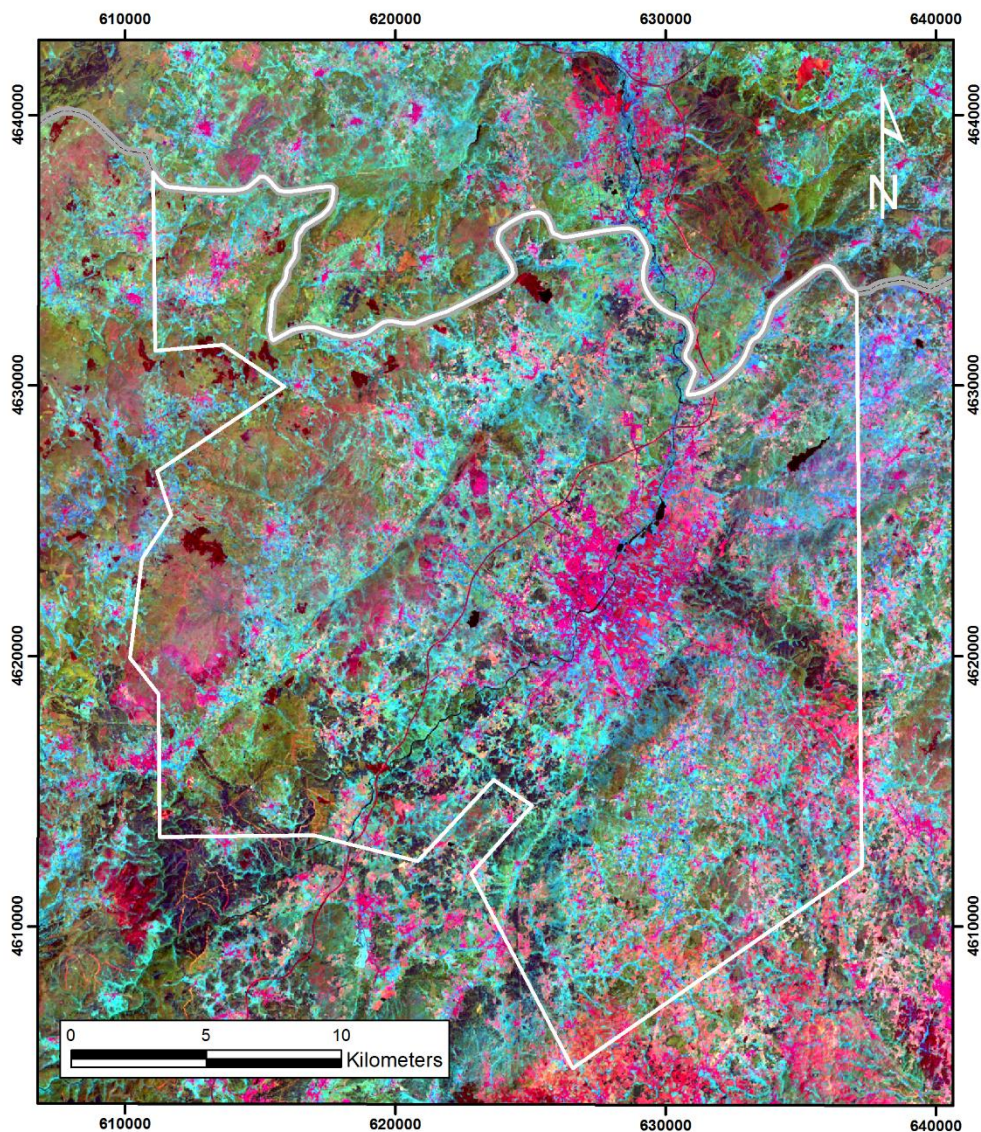


Figure 16 –Band ratio of 4/2, 6/7, 5, in RGB. Outcrops are identified as rose and light brown, vegetation as light blue and water as black. Urbanized areas are highlighted as strong rose.



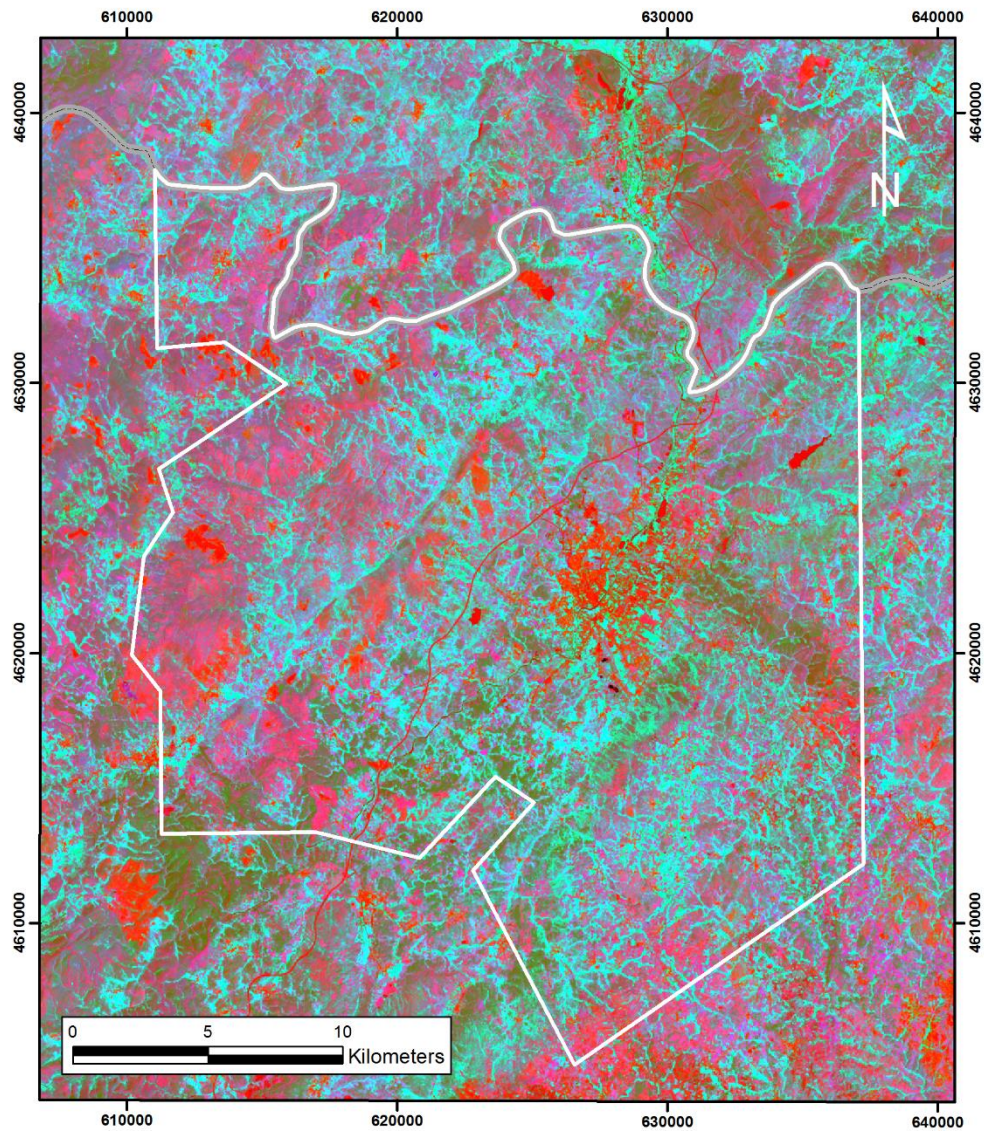


Figure 17 - Kaufmann ratio (7/5, 5/4, 6/7). This band ratio combination highlight metasediments as dark green and granite outcrops are represented as rose, vegetation as light blue and water as red. Some red areas can be related to the hydrothermal alteration.

Vegetation density is a limiting factor when detecting and mapping hydrothermal altered rocks by band rationing. In order to minimize this limitation a spectral unmixing technique, as Principal Component Analysis, is applied.

### 5.1.3. Principal Component Analysis (PCA)

Firstly, this analysis was applied to the six Landsat 8 bands (2, 3, 4, 5, 6, and 7) that output an eigenvector matrix, represented in Table 5. This result allowed to identify which PC contains more useful spectral information from Landsat 8 bands which has much higher contrast than the original bands.

Table 5 - Eigenvectors and eigenvalues of PCA on Landsat 8 imagery.

	PC1	PC2	PC3	PC4	PC5	PC6
BAND 2	0,33541	0,44101	0,47773	-0,53674	0,17977	-0,37997
BAND 3	0,32237	0,31849	0,27952	0,08211	-0,11697	0,83432
BAND 4	0,30589	0,34953	0,05763	0,66891	-0,42059	-0,39573
BAND 5	0,60051	-0,73032	0,29534	0,10042	0,07808	-0,05112
BAND 6	0,45833	0,01101	-0,63896	-0,43077	-0,44251	0,01313
BAND 7	0,34545	0,22004	-0,44139	0,24917	0,75841	0,01221
EIGENVALUES	0,06686	0,00279	0,00102	0,00004	0,00002	0
PERCENT OF EIGENVALUES	<b>94,5305</b>	<b>3,9425</b>	<b>1,4443</b>	<b>0,0549</b>	<b>0,0227</b>	<b>0,0051</b>
ACCUMULATIVE OF EIGENVALUES	94,5305	98,473	99,9173	99,9722	99,9949	100

The sign and magnitude of eigenvector loadings in each PC correspond to the spectral properties of surface materials such as rock, vegetation, and soils (Crosta and Moore, 1989)

PC1 explains 94,5% of the total variance of the data, as shown in table 5. This PC is composed of positive values of all 6 bands and is being responsible for the overall scene brightness. PC2 contains 3.9% of the original data variance and PC3 represents just 1,4%.

The firsts three PC that contain the most data variance was combined in a RGB composite (Figure 18) and it is useful for lithological mapping purposes. Green-yellow colours represents granite outcrops, while blue colour represent metasediments; purple represent vegetation and light blue water bodies. Light green areas highlight hydrothermally altered rocks.

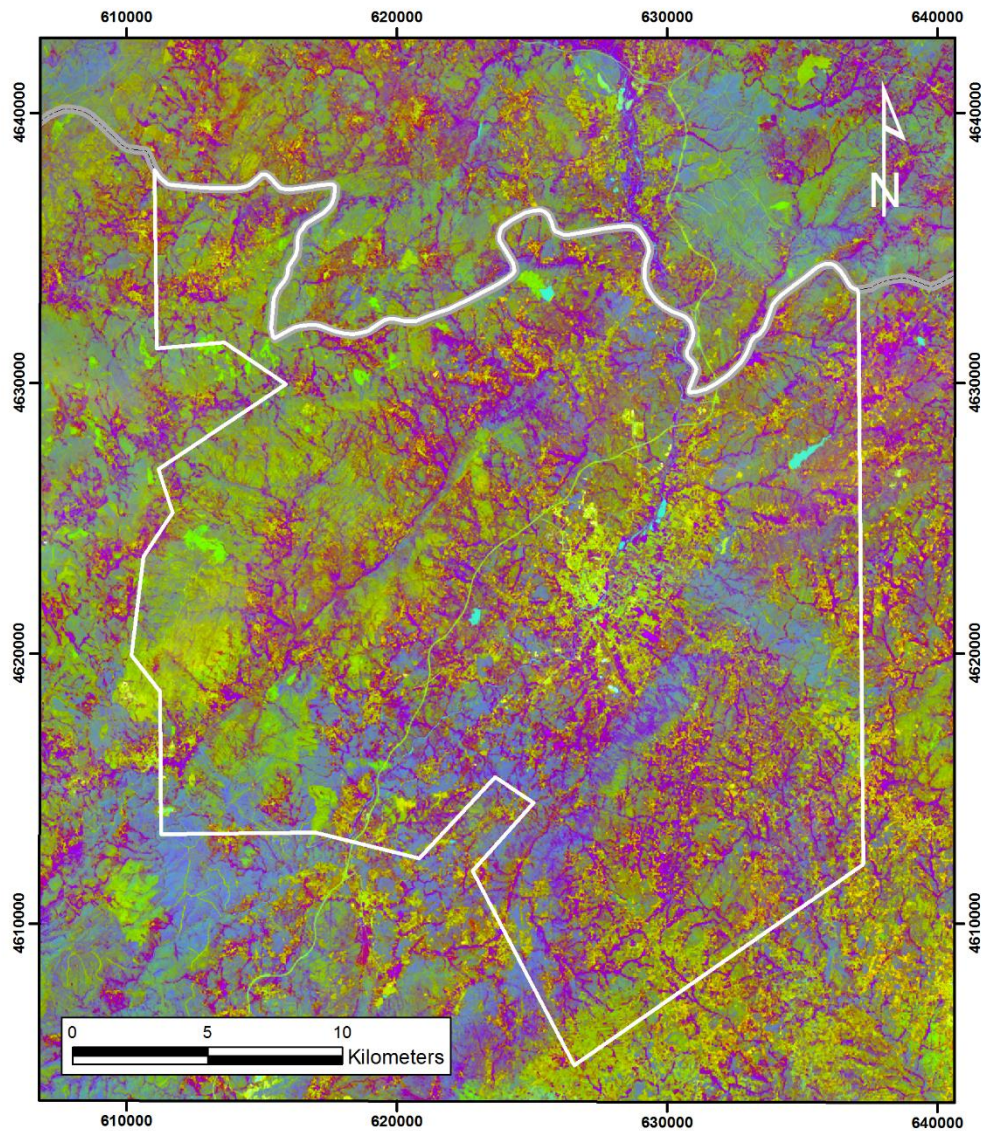


Figure 18 - RGB colour combination of Principal Component Analysis 1, 2, 3 components. Green-yellow colours represent granite outcrops, vegetation in purple, water as light blue and metasediments as blue.

In this study, it was carried out the Crosta technique (Crosta and Moore, 1987), where the Eigenvector statistics output of PCA was analysed in way to identify the PC that contains the spectral information of the target minerals. These selected PC images could then show the targeted minerals by highlighting them as bright or dark pixels, according to the magnitude and sign of the Eigenvector Loadings.

For mapping iron oxides, Landsat 8 bands 2, 4, 5, and 6 were used and for hydroxyl bearing minerals Landsat 8 bands 2, 5, 6, and 7 were used. Eigenvectors and eigenvalues loadings for this iron oxides and clay minerals are shown in Table 6 and 7.

The eigenvector matrix was analysed allowing the identification of PC that contains spectral information, in comparison with the theoretical signatures (reflection and absorption bands) of iron oxides and hydroxyl bearing minerals (Figure 9).

Table 6 presents the loadings resulted from PCA of Landsat 8 bands 2, 4, 5, and 6 for iron oxide minerals enhancement. The PC1 show the entire eigenvectors loading positive. This corresponds to the albedo image with 94,5% of variance data. PC2 with 4,1% of variance represents the vegetated areas as darker pixels. PC3 represent the contrast of SWIR band between the visible and NIR bands. PC4 indicates high positive eigenvector loadings for band 2 (-0,50987) and high negative eigenvector loadings for band 4 (0,81364). Iron oxides minerals have absorption features (low reflectance) of 0.45-0.51  $\mu\text{m}$  (Band 2) and reflectance features (low absorption) of 0.64-0.67  $\mu\text{m}$  (band 4). These two bands have higher loadings in PC analysis, and the pixels with more abundance of iron oxides minerals can be identified as bright pixels in PC4 image (Figure 19).

Table 6 – Eigenvectors and eigenvalues for Principal Components of Landsat 8 bands 2, 4, 5, and 6 for iron oxides minerals.

	<b>PC1</b>	<b>PC2</b>	<b>PC3</b>	<b>PC4</b>
BAND 2	0,37534	0,58755	0,50392	-0,50987
BAND 4	0,34231	0,46945	0,02092	0,81364
BAND 5	0,68836	-0,64727	0,31855	0,07567
BAND 6	0,5178	0,12424	-0,80259	-0,26889
EIGENVALUE	0,05206	0,00225	0,00074	0,00004
PERCENT OF EIGENVALUES	<b>94,4995</b>	<b>4,0905</b>	<b>1,3445</b>	<b>0,0654</b>
ACCUMULATIVE OF EIGENVALUES	94,4995	98,5901	99,9346	100

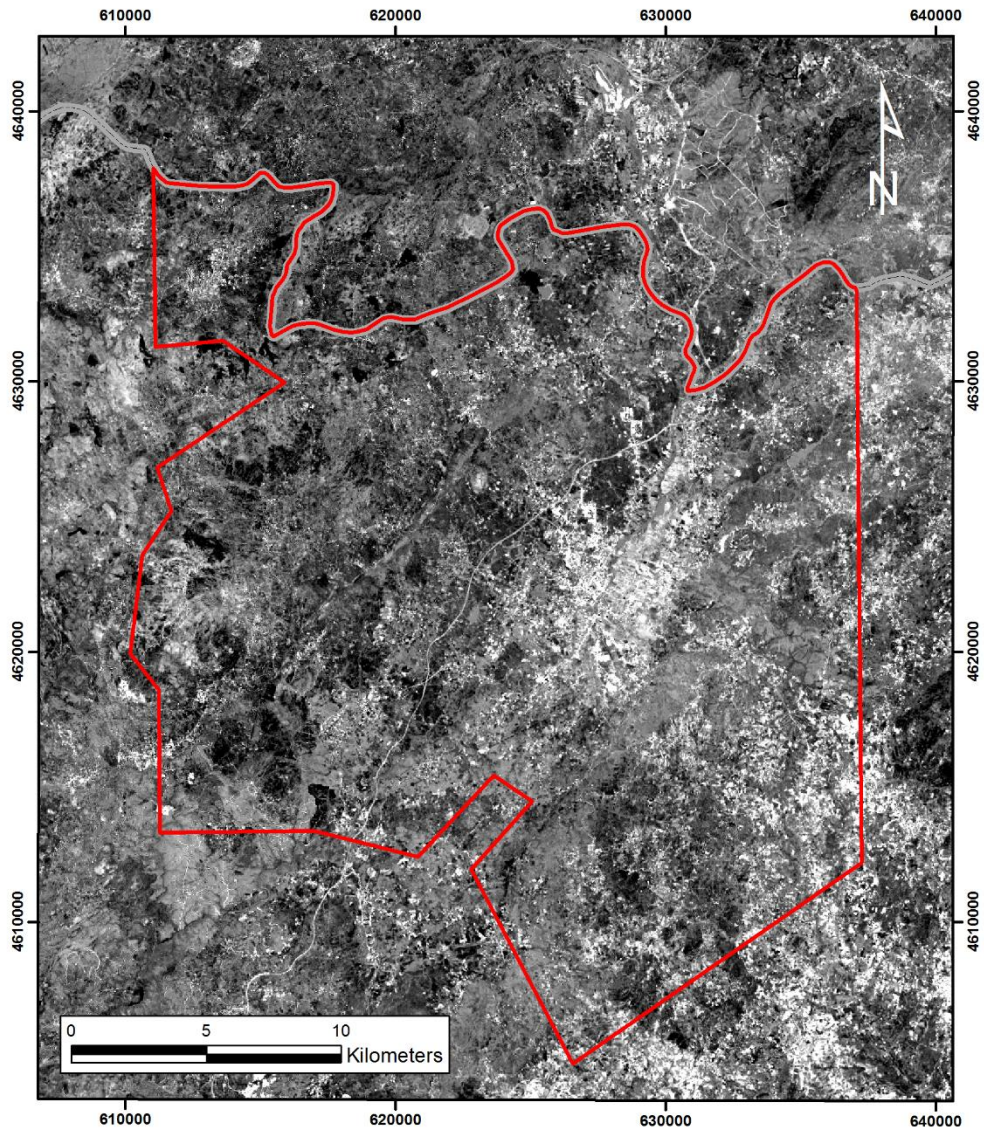


Figure 19 – Principal Component image from Landsat 8 data for iron oxides minerals (PC4) as bright pixels.

Hydroxyl-bearing minerals have reflectance features of 1.55-1.75  $\mu\text{m}$  (band 6) and absorption of 2.1-2.4 $\mu\text{m}$  (band 7). Analysing the Table 7, PC1 have all the eigenvectors loading positive whereby the albedo image has 94,8% of data variance. PC2 indicates strongly vegetated areas in dark pixels with a percentage of variance of 3,6%. PC3 describes the contrast between SWIR bands and visible/NIR bands. PC4 highlights hydroxyl bearing minerals as dark pixels. PC4 show negative eigenvector loading for band 7 and positive eigenvector loading for band 6. This means that clay minerals have absorption in band 7 and reflection in band 6. It was expected that these eigenvectors has opposite signs. Thus, hydroxyl bearing minerals are mapped as dark grey to black

pixels in PC4 image. In order for hydroxyl bearing minerals to be mapped in brighter tones, an inverse of PC4 (DN multiplied by -1) was created (Figure 20).

Table 7 - Eigenvectors and eigenvalues for Principal Components of Landsat 8 bands 2, 5, 6, and 7 for Hydroxyl bearing minerals.

	PC1	PC2	PC3	PC4
BAND 2	0,36665	0,53434	0,74238	-0,17007
BAND 5	0,67660	-0,70004	0,19641	0,11657
BAND 6	0,51130	0,23570	-0,56116	-0,60673
BAND 7	0,38257	0,41095	-0,30885	0,76770
EIGENVALUE	0,05383	0,00206	0,00088	0,00002
PERCENT OF EIGENVALUES	<b>94,78520</b>	<b>3,62800</b>	<b>1,54620</b>	<b>0,04060</b>
ACCUMULATIVE OF EIGENVALUES	94,78520	98,41310	99,95940	100,00000

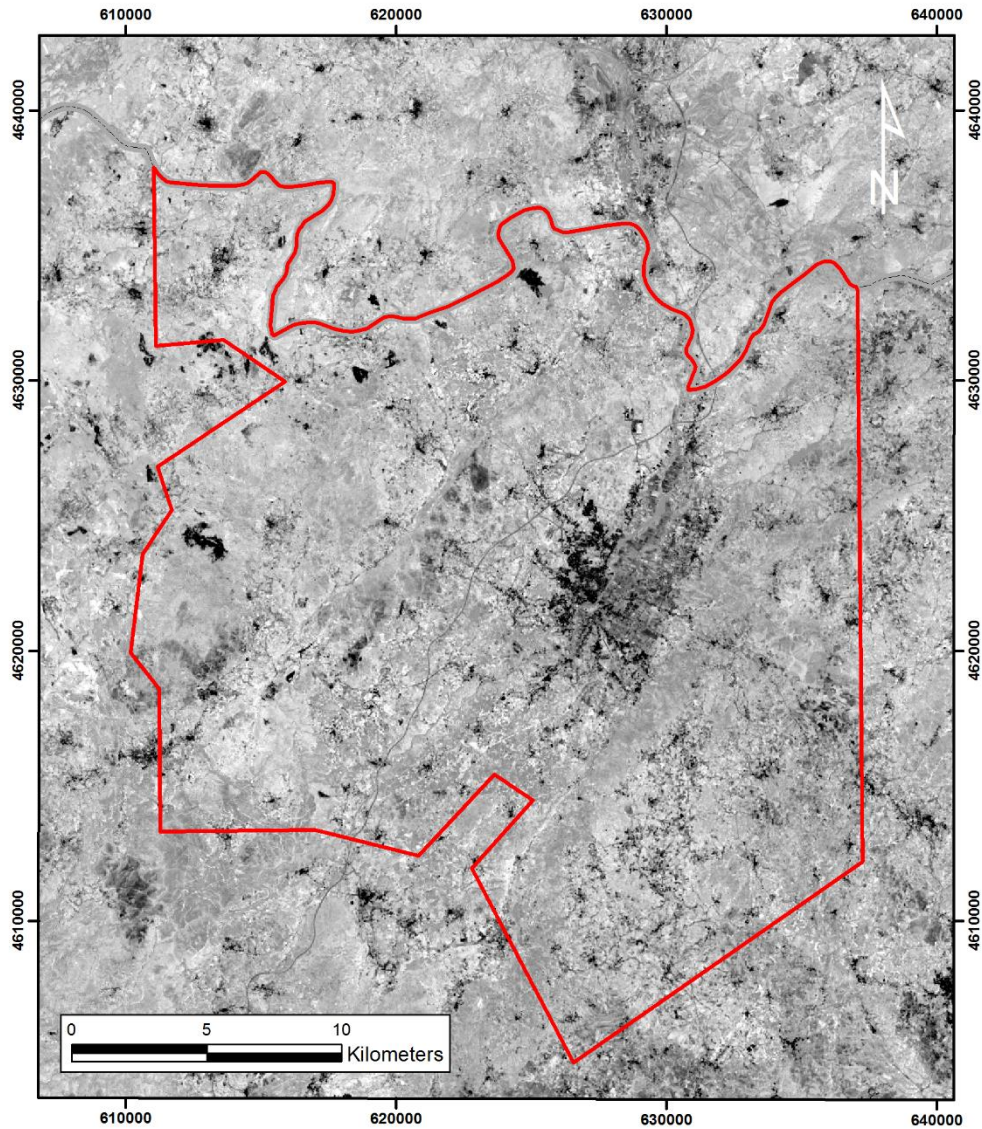


Figure 20 - Principal Component image from Landsat 8 data for hydroxyl bearing minerals (PC4) as bright pixels.

An image displaying pixels with anomalous concentration in hydroxyl and iron oxides bearing minerals as brightest pixels was created by merging of hydroxyl bearing image and iron oxide bearing image, by using Crosta technique. This new image was combined with the other two in a RGB composite (Iron oxide bearing image, iron oxide and hydroxyl bearing image, hydroxyl bearing image). A colour image resulted where bright pixels within alteration zones are areas where both iron stained and argillized; bright reddish to dark orange correspond to areas more argillaceous than iron stained; bright cyan to bluish zones are more iron stained than argillized (Figure 21).

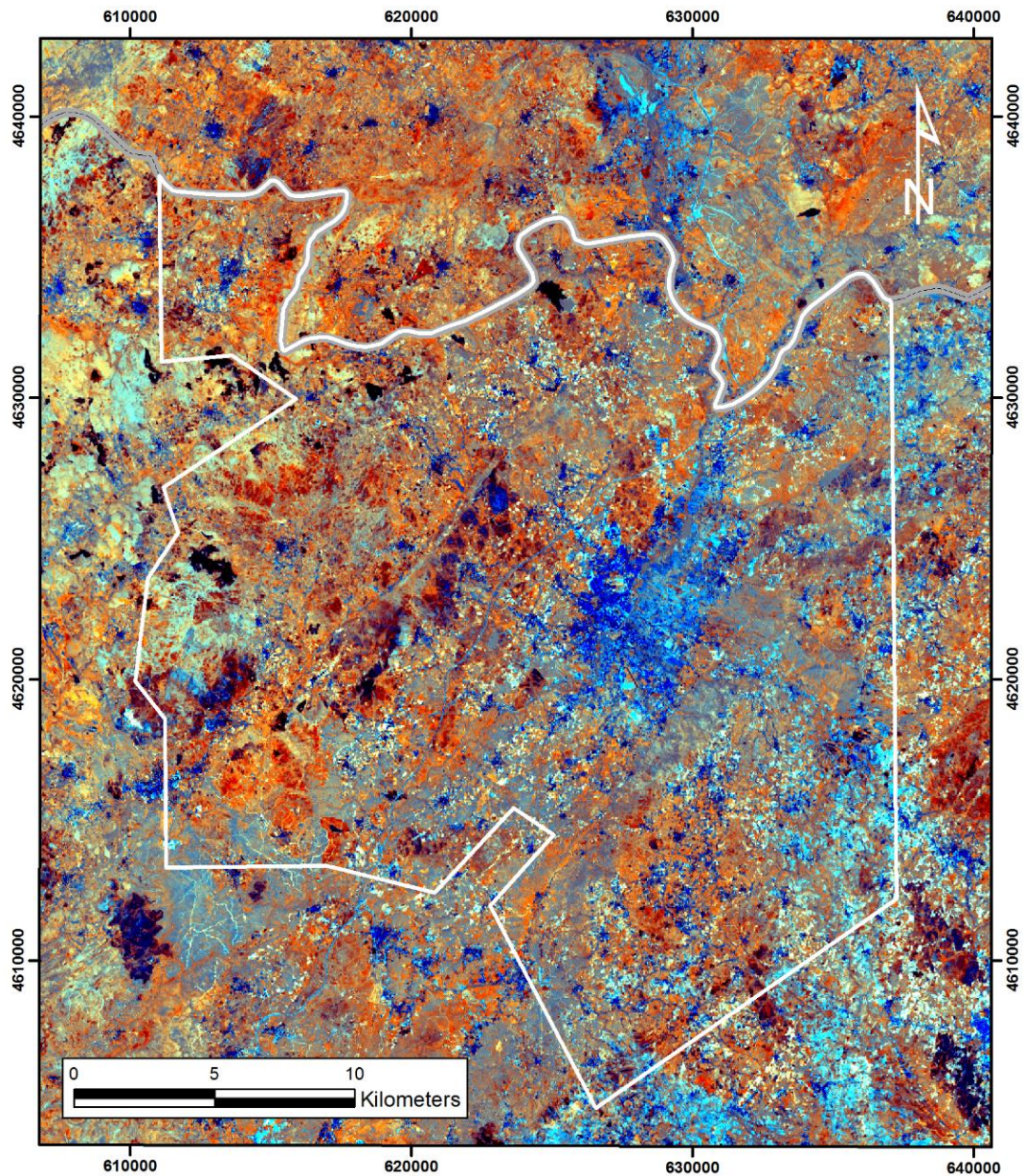


Figure 21 – RGB combination using hydroxyl bearing image, hydroxyl and iron oxide bearing image, and iron oxide bearing image. This composite map the hydrothermal alteration areas.

## 5.2. Feature Extraction

### 5.2.1. Lithologic Mapping

Mapping lithology using remote sensing techniques consists in spectral reflectance differences of the lithology present in the studied area. In this study a regional lithological map was created using the images that result from the methods applied above (Band combination, band ratio and PCA).



Some single band combinations demonstrated useful in lithological mapping. The true colour composite images (Figure 10) simulate a photograph where the colours are similar to those visualized by human eye, and allow the identification of some outcrops. Initially a false infrared image (Figure 11) was used to discriminate vegetation cover from rock outcrops. Vegetated areas showed in red, are mostly along the streams. Enhanced images allow good discrimination of the different lithology present in this area. Visual analysis of Figure 12, a contrast-enhanced image (RGB 7, 5, 2), shows in light green vegetation, granitoids in rose to red colour, and metasediments in dark green. Another false colour composite that enhances lithological feature is the RGB (5, 6, 7) (Figure 13). This figure allows the identification of granitoids as light blue colour, metasediments as brown. However these images do not distinguish so well between different lithologies, because of the topography and other interferences, being difficult to define contacts.

Band ratios revealed a good technique in lithologic mapping, since this method cancels illumination differences from topography, sun shadowing and others. Some band ratio, such as Sabin's ratio (Figure 15) show granitoids in green to yellow colour and dark blue for metasediments. Vegetated areas are represented as light green and urbanized areas as light pink. Kaufmann ratio (Figure 17) represents the granitoids as rose to red colour and metasediments in dark green.

Figure 18 obtained by PCA of Landsat 8 bands 2-7 contains the three PC with more variance data. This image allows the recognition of different lithologies and alteration. Granitoids are represented as green with yellow and rose tones from minerals of alteration as iron oxides and clays. Metasediments are represented as blue colour. These image was the most useful in define limits and distinguished lithologies.

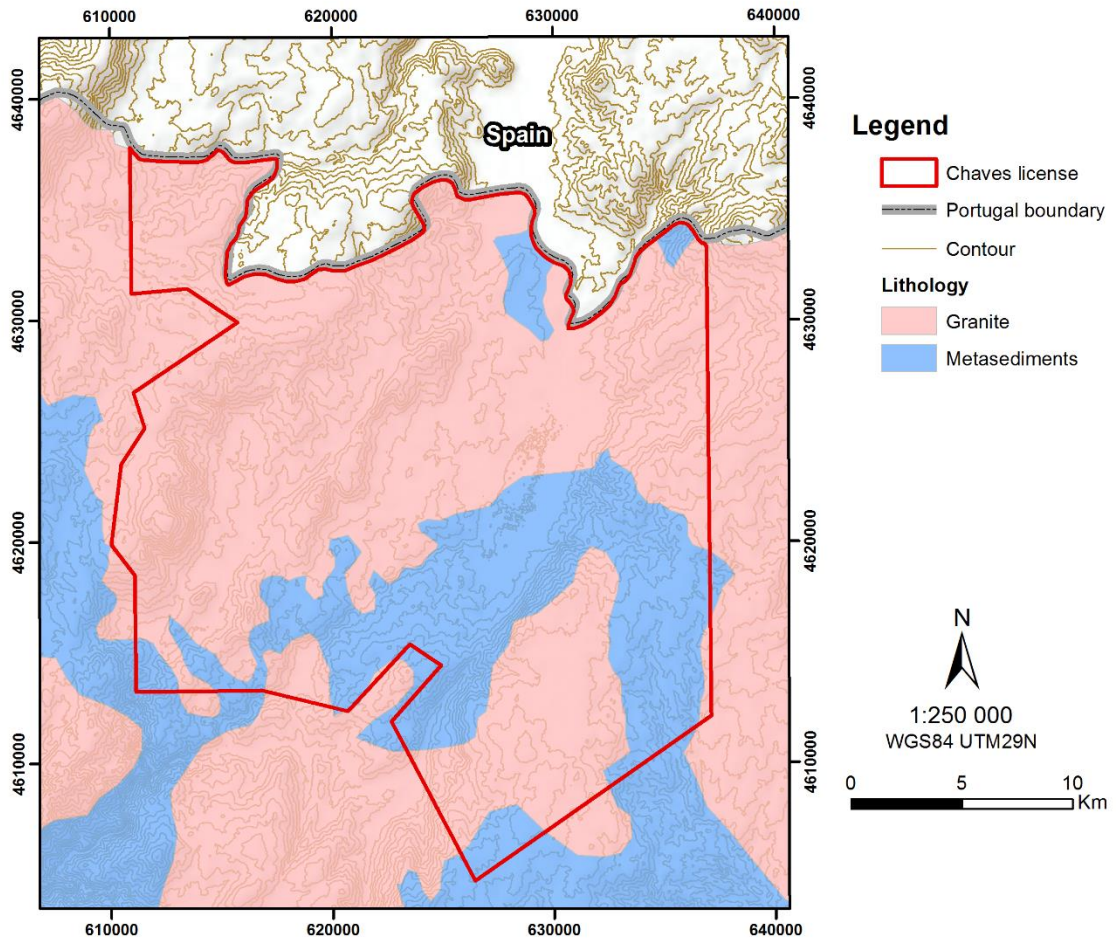


Figure 22 - Lithological map based on Landsat 8 imagery analysis.

The lithological map created (Figure 22) based on Landsat 8 imagery analysis showed be effective in a basic lithological mapping that can be useful in a regional study or in a preparation for an unknown area. Basically, granites and metasediments are the constituents of the studied area. The published geological maps show a variety of granites bodies in this region, but Landsat 8 imagery didn't allowed subdivided that. However, some contacts showed on published maps can be identified on Landsat 8 imagery. Sometimes these contacts between granites and metasediments, correspond to geomorphic boundaries, where generally metasediments tend to form lower ground than the granites.

## 5.2.2. Structural Mapping

In this study, geologic and morphologic lineament were extracted based on True Colour composite (Figure 10) and FCC images, as Figure 13 and 15, which enhance these patterns. Stretching grey scale and balance will turn more contrasting some structures difficult to identify in raw images. The use of DEM imagery helped in the extraction of some information, and validates other. The delineation of lineaments was supported with some processing tools such as the creation of a hillshade image, with the definition of the z-factor and the incidence and azimuth of the illumination source.

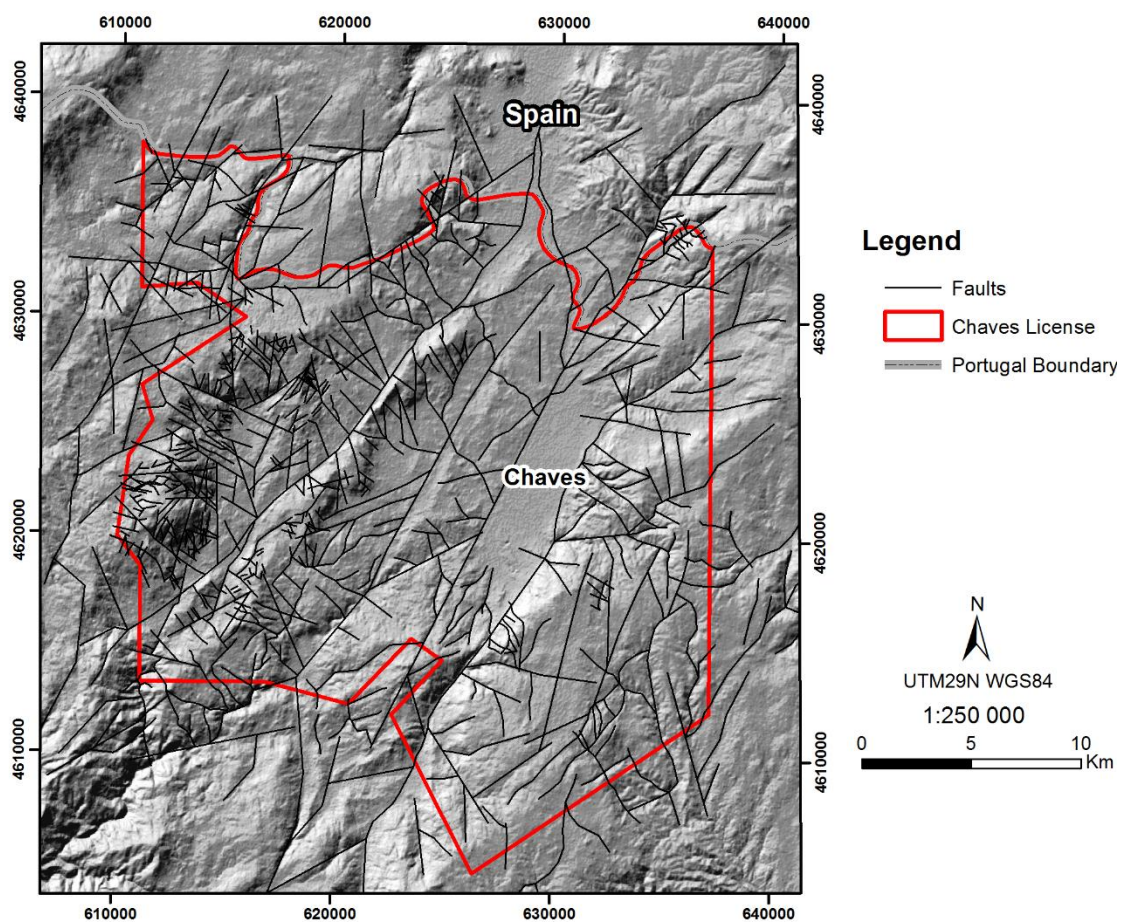


Figure 23 – Structural pattern defined based on Landsat 8 imagery and terrain analysis.

The structural information extracted (Figure 23) consists in parallel northeast trending regional faults that are linked with several east to northeast trending faults, and more locally northwest trending faults link to this major structures. These fracture patterns have an important role as controls on ore deposits acting as conduits of fluids.

### 5.2.3. Hydrothermal Alteration Mapping

In the Chaves license, as known, the geological setting and the auriferous occurrence indicates an association between gold deposits and hydrothermal alteration zones. The known gold bearing quartz veins are within granite rocks that are altered, and are result of chemical interactions with hydrothermal fluids responsible by the gold deposition. This alteration forms a halo around these quartz veins installation areas, providing an exploration target considerably broader than the deposit. Considering this, the spatial distribution of hydrothermally altered rocks can define outflow zones of hydrothermal systems. The delineation of this hydrothermal alteration zones is a great resource for new target areas definition, in gold exploration. In Figure 24 this hydrothermally altered zones were identified based on the results of band ratio and PCA images (Figures 15, 16, and 21).

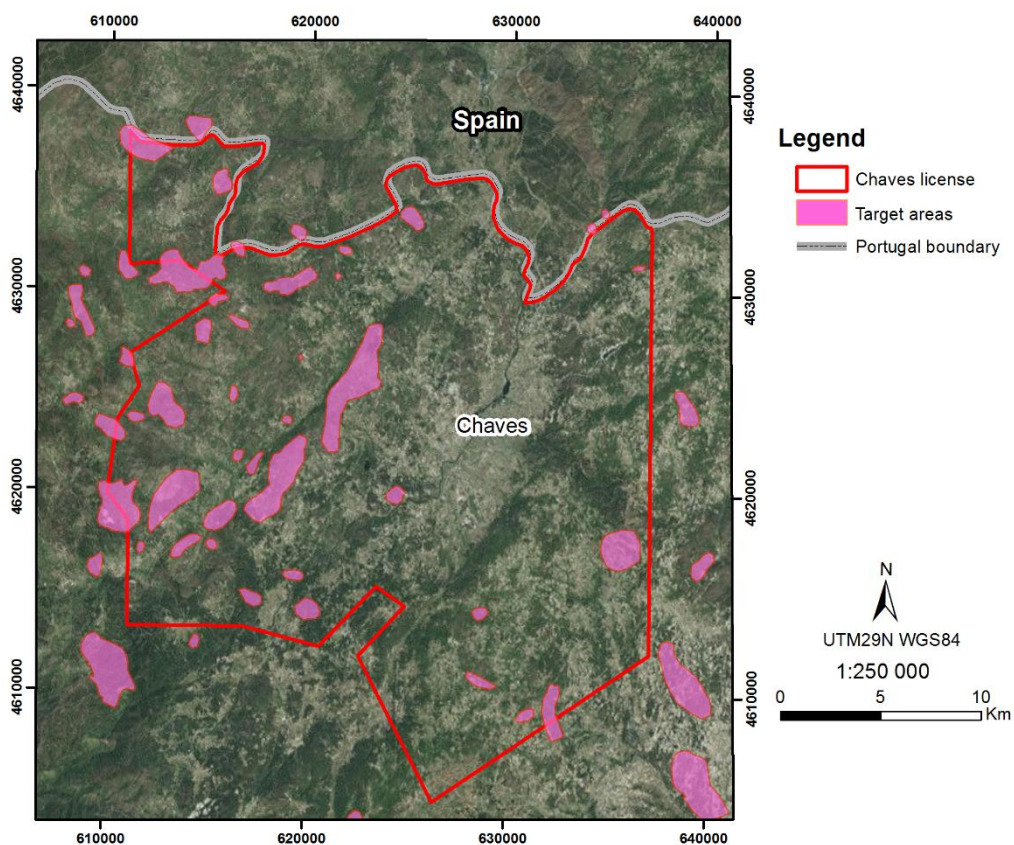


Figure 24 - Hydrothermal alteration areas in and around Chaves license.

These techniques highlight areas where concentration of minerals and assemblage of alteration minerals, as iron-bearing minerals, hydroxyl-bearing minerals

and hydrated sulphates occur, discriminating altered from unaltered rocks. High vegetation density is a limitation on detection of these alteration areas. For a local study is required high resolution imagery to minimize the vegetation effect.

These areas where occurred hydrothermal alteration of the adjacent country rocks can be an indication of vein deposits, but not all ore bodies are accompanied by alteration, and can occur alteration but not associated with mineralization

In way to validate this information, it was compared with historical exploration data, using the anomalous basins determined by Minas Romanas based on BLEG results (Figure 25). This comparison showed that alteration areas identified seems to be related with some gold anomalous basins.

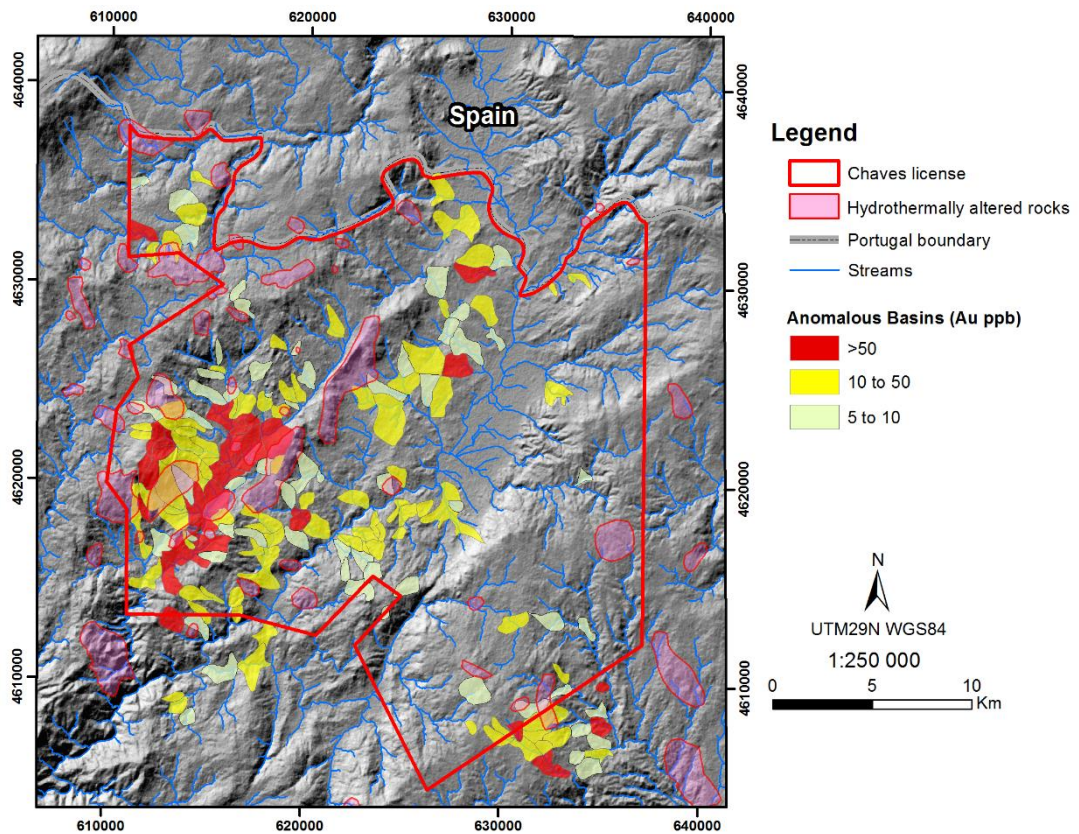


Figure 25 - Hydrothermal alteration map with Au anomalous basins for Chaves License.

### 5.3. Target Exploration Map

A target exploration map was created identifying areas where gold mineralization may possibly occur. This map it was created based on data obtained by Landsat 8 imagery analysis and some geologic assumptions:

- Gold mineralization occurs in syn-D3 two-mica granite;
- Deposits usually occur associated to geologic structures;
- Alteration of the adjacent country rocks can be an indication of mineral deposit.

With the extracted information from Landsat 8 imagery analysis, it was possible to combine lithological information with the structural and the hydrothermally altered areas. The combination of this data has defined new exploration targets, with a higher possibility of gold deposit occurrence, backed by historical data (BLEG study) and field observations (Figure 26).

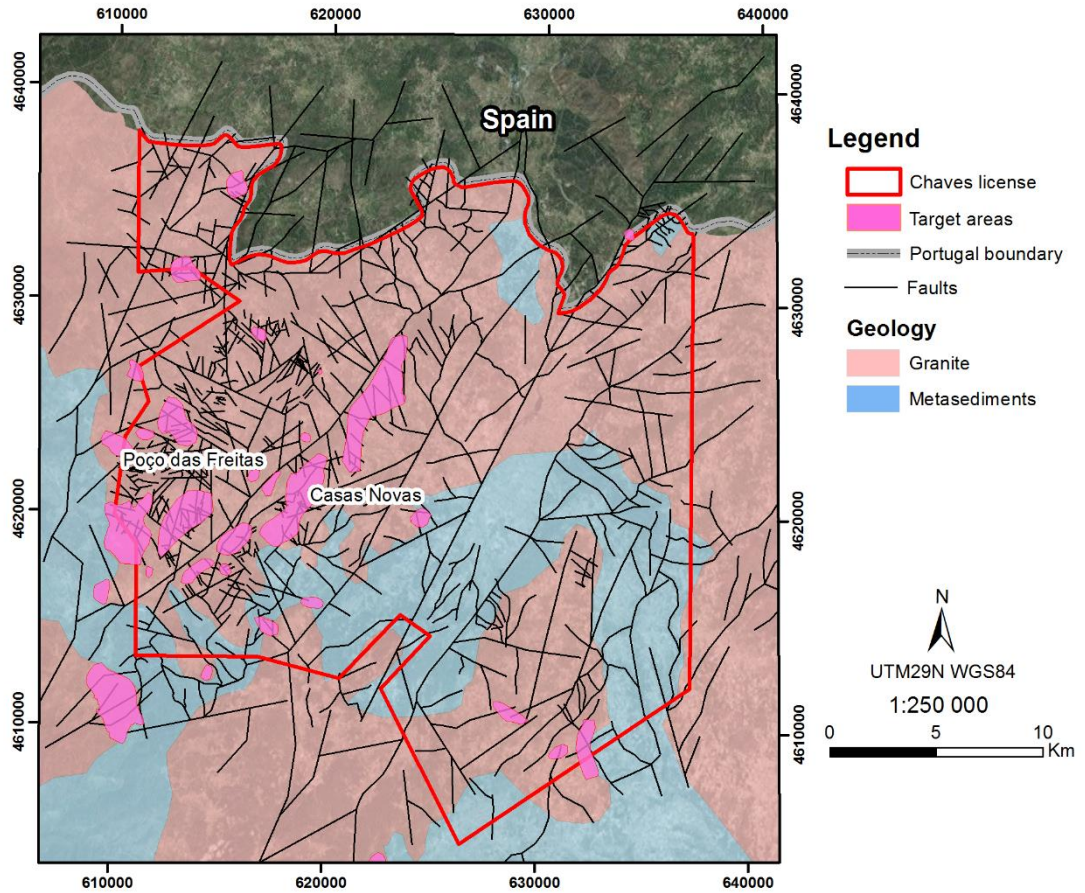


Figure 26 - Target exploration map

Some known places of mineralization were not identified in this study, as Limarinho. This can be justified by the dense vegetation cover combined with the Landsat 8 image resolution. Other areas as Poço das Freitas or Casas Novas are known areas where occur mineralization and was highlighted in this study.

## 6. Conclusions

In greenfield projects remote sensing can be a useful technique to apply in order to define initial exploration targets. In vast areas like Chaves license, a remote sensing study is an essential aid to identify fracture patterns that may have been used as conduits for Au-bearing fluids and highlight hydrothermally altered rocks that can be associated with gold deposits.

Remote sensing can provide information that is not otherwise available to a geologist and it is an effective tool to apply during exploration target generation. These techniques are helpful for areas that are inaccessible and without geological maps. In addition, some geological structures and mineral alteration can only be seen from satellite imagery on a regional scale. This is relevant to cover areas where the geologist interpolates the data, but in areas like the Chaves license, the application of remote sensing techniques have the problem of vegetation and urbanized areas. A revised and more detailed remote study would require a higher spatial resolution imagery.

The analysis of Landsat 8 imagery in this study showed that is effective in data extraction for lithologic information, structural patterns and highlighting hydrothermal alteration. The target exploration map is obtained by the combination of remote sensing information and other geological data and shows the areas with potential for gold occurring and can be used in the further exploration works through the region to discover new anomalous zones.





## 7. Further Work

In continuation of this study, some of these new found targets should be validated on field and a supervised classification can be carried out based on field measurements. Considering the potential of the remote sensing in mineral exploration and to continue generating targets, this techniques can be applied to surrounded areas to the Chaves license, helping on identification of hydrothermally altered rocks where possibly can occur gold mineralization.

For a better definition of the targets generated with this study, can be analyzed high-resolution imagery, which certainly will highlight hydrothermally altered minerals with more confidence. Also, with a better imagery resolution, signal detection in vegetated areas it will be more efficient.

Other remote sensing techniques can be tested and different types of imagery used, in way to help the exploration programs and support the works on the field.



## 8. References

- Ali, A., & Pour, A., 2014. Lithological mapping and hydrothermal alteration using Landsat 8 data: a case study in ariab mining district, red sea hills, Sudan. *International Journal of Basic and Applied Sciences*, 3(3), 199–208.
- Allan, J. C., 1965. A mineração em Portugal na antiguidade. *Bol. Minas*, Lisboa. 2 (3): 139/175. 1965. Direcção-Geral de Geologia e Minas.
- Baker, T., Pollard, P. J., Mustard, R., Mark, G. & Graham, J. L., 2005. A comparison of granite-related tin, tungsten, and gold-bismuth deposits: Implications for exploration. *Society of Economic Geologists Newsletter*, nr. 61, pp.5-17.
- Boiron, M. C., Cathelineau, M., Banks, D. A., Yardley, B. W. D., Noronha, F. & Miller, M. F., 1996. P-T-X conditions of late Hercynian fluid penetration and the origin of granite-hosted gold quartz veins in northwestern Iberia: As multidisciplinary study of fluid inclusions and their chemistry. *Geochimica et Cosmochimica*, 60 (1), pp. 43-57.
- Cabral, J., 1995. Neotectónica em Portugal Continental. Memórias, 31. Serviços Geológicos de Portugal.
- Carvalho, J. & Ferreira, O., 1954. Algumas lavras auríferas romanas. Estudos Notas e Trabalhos, IX (1-4), pp. 20-46.
- Cepedal, A., Martínez-Abad, I., Fuertes-Fuente, M. & Lima, A., 2013. The Presence of Plumboan Ingodite and a Rare Bi-Pb Tellurosulfide,  $Pb_3 Bi_4 Te_4 S_5$ , in the Limarinho Gold Deposit, Northern Portugal. *The Canadian Mineralogist*, 51, pp. 643-651.
- Clark, R.N., Swayze, G.A., Wise, R., Livo, E., Hoefen, T., Kokaly, R. & Sutley, S.J., 2007. USGS digital spectral library splib06a: U.S. Geological Survey, Digital Data Series 231. <http://speclab.cr.usgs.gov/spectral-lib.html>. Accesed Aug. 2015
- Claverol, M. G., Luque, C. & Suarez, V., 1987. El lineamento tectónico Nazaré (W de Portugal) - Luarca (NW de España) y su implicación metalogénica (Macizo Hespérico). In: Geol. de los granitoides y rocas asociadas del Macizo Hespérico. Libro Homenaje a L. C. Garcia de Figuerola. Editorial Rueda, Salamanca, pp. 447-455.

- Climate-Data.org, 2014. Clima: Chaves. [ONLINE] Available at: <http://pt.climate-data.org/location/7128/>. [Accessed 31 August 15].7
- COGEMA, 1990. Sector de Poço das Freitas. Relatório de trabalhos, Setembro de 1990, 49p. (Relatório não publicado).
- Crosta, A. P. & Rabelo, A., 1993. Assessing of Landsat TM for hydrothermal alteration mapping in central western Brazil . Proceedings of Ninth Thematic conference geologic remote sensing Pasadinea, p. 1053-61, California, USA.
- Dias, R. & Ribeiro, A., 1993. Porto–Tomar shear zone, a major structure since the beginning of the Variscan orogeny. *Comun. Inst. Geol. Min.*, Lisboa. 79, pp.31-40.
- Dias, R. & Ribeiro, A., 1995. The Ibero-Armorican arc: a collision effect against an irregular continent? *Tectonophysics*. 246, pp.113–128.
- Dias, R., 2010. Evolução geodinâmica de Portugal no contexto do ciclo Varisco. *VIII Congresso Nacional de Geologia*. GEOTIC – Sociedade Geológica de Portugal. e -Terra. Volume 8–nº 3
- Drury, S. 2001. Image Interpretation in Geology. Blackwell Science, 290p. USA.
- Ferreira, N., Iglésias, M., Noronha, F., Pereira, E., Ribeiro, A. & Ribeiro, M. L., 1987. Granitóides da zona Centro Ibérica e seu enquadramento geodinâmico. In: *Geología de los Granitóides y Rocas Asociadas del Macizo Hesperico*. Libro de Homenaje a L. C. García de Figuerola, Editorial Rueda. Madrid
- Fernández, F.J., Chaminé, H.I., Fonseca, P.E., Munhá, J.M., Ribeiro, A., Aller, J., Fuertes-Fuentes, M., Borges, F.S., 2003. High-temperature fabrics in garnetiferous quartz-tectonites from W Portugal: geodynamic implications for the Iberian Variscan Belt. *Terra Nova* 15, 2, pp. 96–103.
- Julivert, M., Fontboté, J.M., Ribeiro, A. & Conde, L.E.N., 1974. Mapa Tectónico de la Península Ibérica y Baleares, Escala 1:1000.000. Memória Explicativa. Instituto Geologico y Minero de España, Madrid.
- Griveaud, P. & Dixsaut, C., 1989. Permis de Poço das Freitas. Etude structurale des zones de Limarinho, Poço das Freitas, Bobadela, 8p. (Relatório não publicado).

- Goetz, A. F. H., Rowan, L. C. & Kingston, M.J. 1982. Mineral identification from orbit: initial results from the Shuttle Multispectral Infrared Radiometer. *Science*, 218, pp. 1020-1031.
- Goetz, A. 2009. Three decades of hyperspectral remote sensing of the Earth: A personal view. *Remote Sensing of Environment*, 113, pp. 5-16.
- Goldfarb, R.J., Groves, D.I. & Gardoll, S., 2001. Orogenic gold and geologic time: A global synthesis. *Ore Geology Reviews*, 18, pp. 1–75.
- Goldfarb R.J., Baker T., Dube B., Groves D.I., Hart C.J.R. & Gosselin P., 2005. Distribution, Character, and Genesis of Gold Deposits in Metamorphic Terranes. *Economic Geology 100th Anniversary Volume*, pp. 407-450.
- Gouanvic, Y., Courrioux, G. & Ovejero, G., 1981. Controle structural de la repartition des indices d'or filoniens du Nord-Ouest de la Peninsule Iberique. *Cuadernos Geologia Ibérica*, 7, pp. 353-367.
- Groves, D.I., 1993. The crustal continuum model for late-Archaean lode-gold deposits of the Yilgarn Block, Western Australia. *Mineralium Deposita*. 28, pp.366–374.
- Groves, D. I., Ridley, J. R., Bloem, E. M. J, Gebre-mariam, M., Hagemann, S. G., Hronsky, J. M. A., Knight, J. T., McNaughton, N. J., Ojala, J., Vielreicher, R. M., McCuaig, T. C. & Holyland, P. W., 1995. Lode-gold deposits of the Yilgarn block: products of Late Archean crustal-scale overpressured hydrothermal systems. In: Coward, M.P., and Ries, A.C., eds., *Early Precambrian Processes*. Geological Society, London, Special Publication. 85, pp.155 -172.
- Groves, D.I., Goldfarb, R.J., Gebre-Mariam, M., Hagemann, S.G. & Robert, F., 1998. Orogenic gold deposits: A proposed classification in the context of their crustal distribution and relationship to other gold deposit types. *Ore Geology Reviews*. v. 13, pp. 7–27.
- Han, T. & Nelson, J., 2015. Mapping hydrothermally altered rocks with Landsat 8 imagery : A case study in the KSM and Snow field zones , northwestern British Columbia. In: Geological Fieldwork 2014, British Columbia Ministry of Energy and Mines, British Columbia Geological Survey Paper, 2015-1, pp.103-112.
- Harford, P., Plimer, I. & Silva R., 1998. Minas Romanas Annual Report, 74 p. (Relatório não publicado).

- Hung, L. Q., Batelaan, O. & De Smedt, F., 2005. Lineament Extraction and Analysis, Comparison of LANDSAT ETM and ASTER Imagery. Case Study: Suoimuoi Tropical Karst Catchment, Vietnam. *Remote Sensing for Environmental Monitoring, GIS Applications, and Geology*. Vol. 59830T-1.
- Hunt, G.R. 1977. Spectral signatures of particulate minerals, in the visible and near-infrared. *Geophysics*, 42, pp. 501-513.
- Inverno, C. M. C., 2011. Comparação de jazigos de ouro do tipo orogénico (mesotermiais) e os jazigos de ouro associados a intrusão. Algumas extrapolações para Portugal. *Cuaderno Lab. Xeolóxico de Laxe*. Coruña. Vol. 36, pp. 99-156.
- Julivert, M., Fontboté, J.M., Ribeiro, A., & Conde, L.E.N., 1974. Mapa Tectónico de la Península Ibérica y Baleares, Escala 1:1000.000. Memória Explicativa. Instituto Geologico y Minero de España, Madrid.
- Lima, A., Matias, R., Mendonça, A., 2011. Contribuição para o estudo da Mineração Romana de ouro na Bacia do Rio Terva. In: C.M.B. Martins, A.M.S. Bettencourt, J.I.F.P. Martins, J. Carvalho, (Coords). Povoamento e exploração dos recursos mineiros na Europa Atlântica Ocidental. Centro de Investigação Transdisciplinar "Cultura, Espaço e Memória"/Associação Portuguesa para o Estudo do Quaternário (CITCEM/APEQ), Braga, pp. 241-256
- Lima, A, Rodríguez, R. M., Fonte, & H. Pires, 2014. The Historic Gold Mining in the High Terva River Basin (Northern Portugal). *Comunicações Geológicas*, 101, Especial III, pp. 1289-1293
- Lotze, F., 1945. Zur Gliederung der Varisziden der Iberischen Meseta. *Geotekt. Forsch.* 6, pp.78-92 (traduzido para o espanhol "Observaciones respecto a la division de los variscides de la Meseta Iberica. *Publ. extranjeras sobre geologia de Espana*. 1950. 5, pp.149-166.
- MacKenzie, D. & Craw, D., 2014. Controls on gold mineralization at Valongo, Vila de Rei, Salgueiro, Castromil, Serra da Quinta and Limarinho prospects, northern Portugal. Report to Medgold Resources Corp.
- Markham, B. L. & Helder, D. L., 2012. Forty-year calibrated record of earth-reflected radiance from Landsat: A review. *Remote Sensing of Environment*, 122, pp. 30–40

- Martins, C.B., 2005. A exploração mineira romana e a metalurgia do ouro em Portugal. Tese de Doutoramento, Universidade do Porto (não publicada), 645p.
- Mateus, A. & Noronha, F., 2010. Sistemas mineralizantes epigenéticos na zona centro-ibérica; expressão da estruturação orogénica meso- a tardi-varisca. In: Coteló Neiva, J.M., Ribeiro, A., Mendes Victor, Noronha, F., Magalhães Ramalho, 2010. Ciências Geológicas: Ensino, Investigação e sua História. *Geologia Aplicada*. Volume II. Associação Portuguesa de Geólogos
- Matias, R. (2004). Ingeniería Minera Romana. Elementos de Ingeniería Romana. Congreso Europeo “Las Obras Públicas Romanas”, Tarragona.
- Matte, P., 1986. Tectonics and plate tectonics model for the Variscan belt of Europe. *Tectonophysics* 126, 329 – 374.
- Matte, P., 1991. Accretionary history of the Variscan belt in western Europe. *Tectonophysics* 196, 309 – 337.
- Matte, Ph., 2001. The Variscan collage and orogeny (480-290 Ma) and the tectonic definition of the Armorican microplate: a review. *Terra Nova*. 13, pp.122–128.
- Mendonça, A., 2006. Geoquímica de Ouro na Região de Limarinho (Boticas – Norte de Portugal). Tese de mestrado, Faculdade de Ciências da Universidade do Porto (não publicada), 134 p.
- Mercedes, F., Cepedal, A., Lima, A., Dória, A., Ribeiro, M. A., Guedes, A., 2015. The Au-Bearing vein system of the Limarinho deposit (northern Portugal): Genetic constraints from Bi-chalcogenides and Bi-Pb-Ag sulfosalts, fluid inclusions and stable isotopes. *Ore Geology Reviews*, 72, pp. 213 – 231.
- Mia, M.B. & Fujimitsu, Y., 2012. Mapping hydrothermal altered mineral deposits using Landsat 7 ETM+ image in and around Kuju volcano, Kyushu, Japan. *Journal of Earth System Science*, 121(4), pp. 1049 – 1057
- Moradi, M., Basiri, S., Kananian, A. & Kabiri, K., 2015. Fuzzy logic modeling for hydrothermal gold mineralization mapping using geochemical, geological, ASTER imageries and other geo-data, a case study in Central Alborz, Iran. *Earth Sci Inform*, 8, pp. 197-205



- Mwaniki, M. W., Moeller, M. S., & Schellmann, G., 2015. A comparison of Landsat 8 (OLI) and Landsat 7 (ETM+) in mapping geology and visualising lineaments: A case study of central region Kenya. *ISPRS - International Archives of the Photogrammetry, Remote Sensing and Spatial Information Sciences*, XL-7/W3, 897–903.
- Noronha, F., Ramos, J. M. F., Rebelo, J. A., Ribeiro, A. & Ribeiro, M. L., 1979. Essai de corrélation des phases de déformation hercynienne dans le Nord-Ouest Péninsulaire. *Bol. Soc. Geol. Portugal*, Lisboa. 21 (2/3), pp.227-237.
- Noronha, F. & Ramos, J. M. F., 1993. Mineralizações auríferas primárias no norte de Portugal. Algumas reflexões. *Cuaderno Lab. Xeolóxico de Laxe*. Coruña. Vol. 18, pp. 133-146.
- Noronha, F., Cathelineau, M., Boiron, M. C., Banks, D. A., Dória, A., Ribeiro, M. A., Nogueira, P. & Guedes, A., 2000. A three stage fluid model for Variscan gold metallogenesis in northern Portugal. *Journal of Geochemical Exploration*, 71, pp. 209-224.
- Noronha, F., Ribeiro, M.A., Almeida, A., Doria, A., Guedes, A., Lima, A., Martins, H. C., Sant’Ovaia, H., Nogueira, P., Martins, T., Ramos, R. & Vieira, R. 2006. Jazigos filonianos hidrotermais e aplitopegmatíticos especialmente associados a granitos (norte de Portugal). In: *Geologia de Portugal no contexto da Iberia* (Dias, R. Araujo, A., Terrinha, P. e Kulberg, Editores). Univ.Evora, Evora, 123-138.
- Noronha, F., Ribeiro, M. A., Almeida, A., Dória, A., Guedes, A., Lima, A., Martins, H. C., Sant’Ovaia, H., Nogueira, P., Martins, T., Ramos, R. & Vieira, R., 2013. Jazigos filonianos hidrotermais e aplitopegmatíticos especialmente associados a granitos (norte de Portugal). In: *Geologia de Portugal. Volume I – Geologia Pré-mesozóica de Portugal*. Escolar Editora. 2013.
- Oliveira, J. T., Pereira, E., Ramalho, M., Antunes, M. T. & Monteiro, J. H., 1992. *Carta Geológica de Portugal, escala 1/500 000. 5ª edição*. Serviços Geológicos de Portugal, Lisboa.
- Pereira, E., Ribeiro, A. & Meireles, C., 1993. Cisalhamentos Hercínicos e controlo das mineralizações de Sn-W, Au e U na Zona Centro Ibérica, em Portugal. *Cuaderno Lab. Xeolóxico de Laxe*. Coruña. Vol. 18, pp.89-119.
- Pereira, E. & Meireles, C., 1998. Metais preciosos em Portugal. Situação da investigação Geológica e Mineira. *Estudos Notas e Trabalhos*, 40. Instituto geológico e Mineiro.

- Pereira, E., Ribeiro, A., Marques, F., Munhá, J., Castro, P., Meireles, C., Ribeiro, M. A., Pereira, D., Noronha, F. & Ferreira, N., 2001. Carta Geológica de Portugal, folha 2, escala 1:200 000, Instituto Geológico de Portugal.
- Pour, A., & Hashim, M., 2015. Hydrothermal alteration mapping from Landsat-8 data, Sar Chesmeh copper mining district, south-eastern Islamic Republic of Iran. *Journal of Taibah University for Science*, 9, 155-166.
- Ribeiro, A., Antunes, M. T., Ferreira, M. P., Rocha, R. B., Soares, A. F., Zbyszewski, G., Almeida, F. M., Carvalho, D. & Monteiro, J. H. (1979). *Introduction à la géologie générale du Portugal*, 114 p. Serviços Geológicos de Portugal, Lisboa. (XXVI Congr. Internat. Géol., Paris, 1980).
- Ribeiro, A., Quesada, C. & Dallmeyer, R.D., 1990. Geodynamic evolution of the Iberian Massif. In: Dallmeyer, R.D., Martínez-García, E. (Eds.). *Pre-Mesozoic Geology of Iberia*. Springer Verlag, Berlin, pp. 397–410.
- Ribeiro, A., Pereira, E., Chaminé, H. I. & Rodrigues, J., 1995. Tectónica do megadomínio de cisalhamento entre a Zona de Ossa-Morena e a Zona Centro-Ibérica na região de Porto-Lousã. In: Sodrê Borges, F., Marques, M. *Mem. Mus. Lab. Min. Geol. Fac. Ciênc. Univ. Porto*, 4, pp. 299-303.
- Ribeiro, A., Munhá, J., Dias, R., Mateus, A., Pereira, E., Ribeiro, L., Fonseca, P., Araújo, A., Oliveira, T., Romão, J., Chaminé, H., Coke, C., Pedro, J., 2007. Geodynamic evolution of the SW Europe Variscides. *Tectonics*, 26, pp.1–24
- Sabins, F.F., 1999. Remote sensing for mineral exploration. *Ore Geology Reviews* 14, 157–183.
- Salisbury, J.W., Walter, L.S., Vergo, N., 1989. Availability of a library of infrared (2.1–25.0  $\mu\text{m}$ ) mineral spectra. *American Mineralogist* 74, 938–939.
- USGS, 2014. *Landsat 8 (L8) Level 1 (L1) Data Format Control Book (DFCB)*. Department of the Interior, U.S. Geological Survey, Version 8.0, pp.26
- USGS, 2015a. *Landsat 8 (L8) Data Users Handbook*. Version 1.0, pp. 105
- USGS, 2015b. Using the USGS Landsat 8 Product: [http://landsat.usgs.gov/Landsat8\\_Using\\_Product.php](http://landsat.usgs.gov/Landsat8_Using_Product.php). Accessed Aug., 2015

- USGS, 2015c. Frequently Asked Questions about the Landsat Missions: [http://landsat.usgs.gov//L8\\_band\\_combos.php](http://landsat.usgs.gov//L8_band_combos.php). Accessed Aug., 2015
- USGS, 2015d. Landsat Missions Timeline: [http://landsat.usgs.gov//about\\_mission\\_history.php](http://landsat.usgs.gov//about_mission_history.php). Accessed Aug., 2015
- USGS, 2015e. Landsat 8 History: [http://landsat.usgs.gov//about\\_ldcm.php](http://landsat.usgs.gov//about_ldcm.php). Accessed Aug., 2015
- USGS, 2015f. Earth Explorer: <http://earthexplorer.usgs.gov>. Accessed Aug., 2015.
- van der Meer, D. F. 2004. Analysis of spectral absorption features in hyperspectral imagery. *International Journal of Applied Earth Observation and Geoinformation*, 5, 55 – 68.
- Vera, J.A., 2004. *Geología de España*. SGE-IGME, Madrid, 890p.
- VIEGAS L. F. & MARTINS, L.P., 1992. Notas sobre a prospecção do ouro em Portugal. *Estudos, Notas e Trabalhos*, 34, pp. 95-106.
- Vignerresse, J.L., 1999. Intrusion level of granitic massifs along the Hercynian belt: balancing the eroded crust. *Tectonophysics*, 307, pp.277–295
- Sukumar, M., Venkatesan, N. & Babu, N. K., 2014. A Review of Various Lineament Detection Techniques for High Resolution Satellite Images. *International Journal of Advanced Research in Computer Science and Software Engineering*. Volume 4, Issue 3. pp. 72-78



